NSSI Neutron Newsletter

Number 3
June 2023

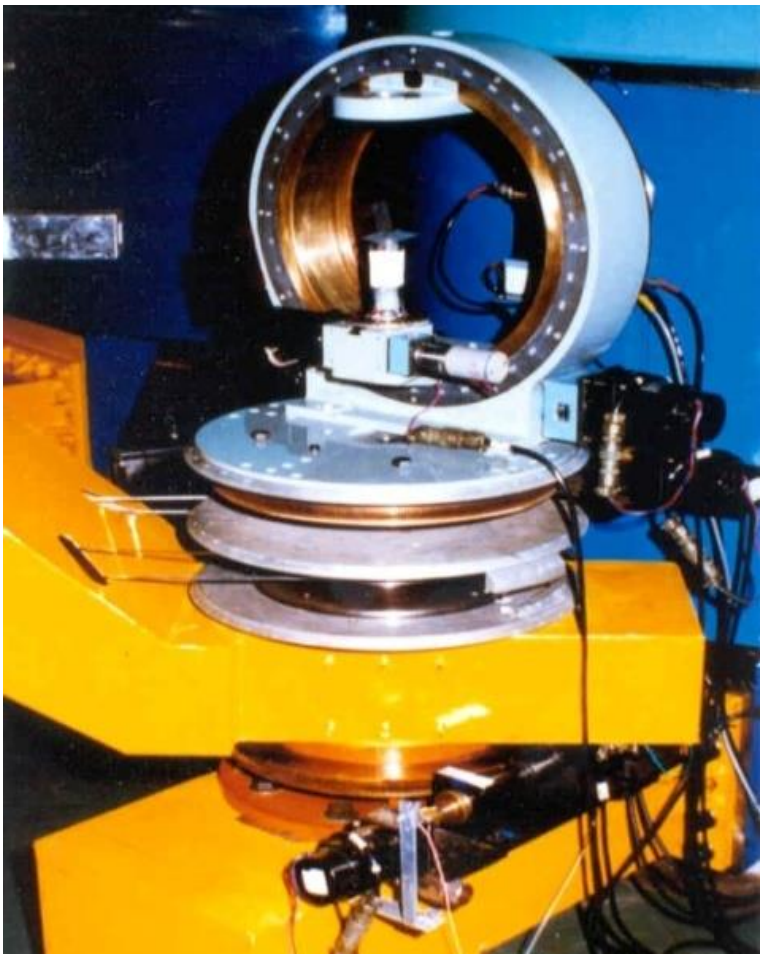

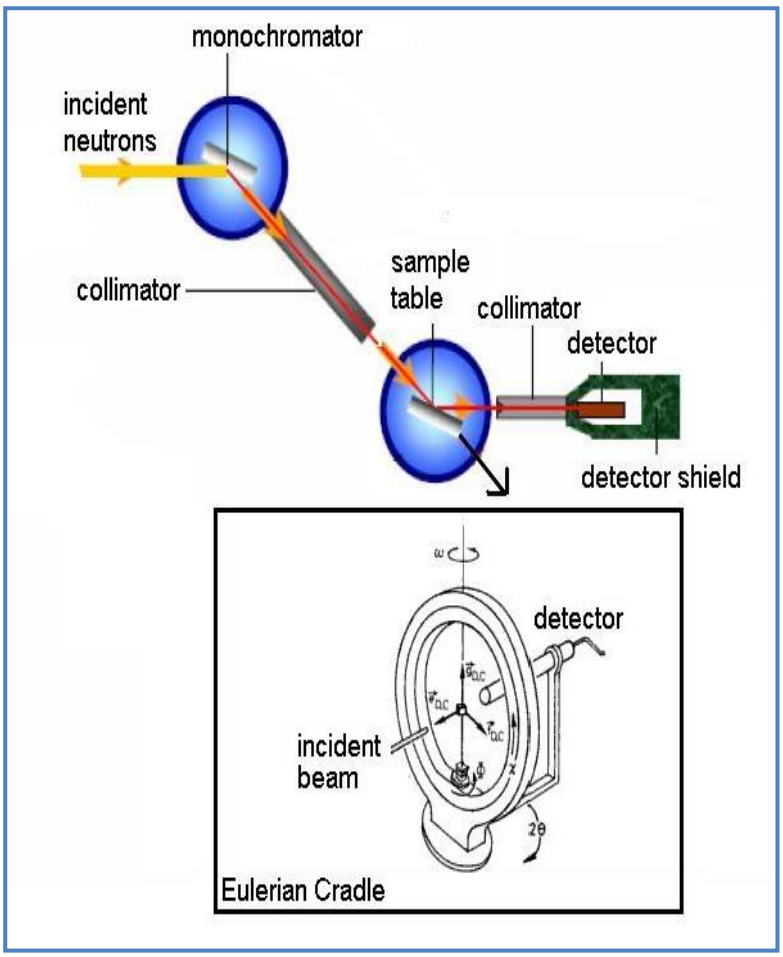

Neutron Scattering Society of India

Neutron Scattering Society of India (NSSI) was formed in 2008 to provide a forum for neutron users for promoting neutron-based research and development activities including applications in the country . The NSSI is the adhering society representing the neutron users in India on the Asia-Oceania Neutron Scattering Association (AONSA), which is an affiliation of all neutron scattering societies in the Asia-Oceania region. NSSI happens to be one of the founder members of the AONSA along with the respective neutron societies from Japan, South Korea, Australia and Taiwan. At present NSSI has about 300 registered members from various universities and institutions spread all over the country.

Cover Page

The four-circle single-crystal diffractometer at Dhruva reactor (left) and the schematic diagram (right). See the article on *Single-crystal Neutron Diffraction at Dhruva: A tool to unravel the crystalline structure at atomic scale* by R. Chitra and Rajul Ranjan Choudhury (page 18).

Contents

Editorial

We are happy to bring out this issue of the NSSI Newsletter. This issue highlights a broad variety of high-quality neutron science done in India, covering both fundamental and applied aspects, in materials science, protein interactions, Li/Na battery materials, and magnetism in different compounds and multilayers. These highlights also emphasize the breadth of neutron scattering techniques being pursued by the scientists in India.

This issue includes a topical review on single-crystal neutron diffraction. The review has two components, first the description of the technique as implemented at the Dhruva reactor, and then an illuminating journey of the single-crystal neutron diffraction research at BARC over the last six decades at the CIRUS and the Dhruva reactors.

We hope the readers will like this issue and contribute excellent highlights of their research to the future issues.

Published by The General Secretary, NSSI.

Message from the President, NSSI

I am extremely delighted to present the June, 2023 issue of NSSI Newsletter. The highlights in this issue give a glimpse of growing interdisciplinary character of research using neutron-based techniques in the country. The 11 highlighted abstracts of research publications are related to a rich variety of problems like spinodal decomposition in alloys, protein gelation, statics and dynamics of battery related materials, exotic low dimensional magnetic phases and multiferroics. The readers may find the short review article on the status of single crystal neutron diffractometer facility at Dhruva Reactor very useful for planning single crystal neutron diffraction work. I take this opportunity to congratulate the Editors for bringing out such an impressive issue within six months of the previous issue.

Dhananjai Pandey
President, NSSI

Reports as sent to AONSA from NSSI

The XIX School on Neutrons as Probes of Condensed Matter (NPCM-2022) has been organized by BARC and UGC-DAE Consortium for Scientific Research, Mumbai in association with NSSI during November 14-19, 2022 in Mumbai, India to enhance awareness about neutron scattering techniques and discuss the recent research in condensed matter physics by neutron scattering. The school has been attended by about 60 participants consisting many PhD students and few faculty members from universities and research institutes in India. The school comprised lectures on basic principles and applications of neutron scattering techniques by expert scientists from BARC and UGC-DAE-CSR, Mumbai. It also consisted tutorials as well as hands on experiments using the neutron scattering facilities at Dhruva reactor, BARC, Mumbai. Prof. Amlan Pal, Director, UGC DAE CSR and Dr. S M Yusuf, Director, Physics Group, BARC, among others, spoke in the inaugural session of the School.

Another important event organized during the NPCM-2022 was 2nd NSSI lecture. It has been delivered (online) by Prof. Brendan Kennedy, The University of Sydney, Australia. He was former President of AONSA and of the Australian Neutron Beam Users Group (ANBUG). He delivered the lecture on "Phase Transitions in Oxides: Using neutron scattering to observe both the obvious and not-so-obvious changes". The session was chaired by Prof. D. Pandey, President NSSI.

During NPCM-2022, the annual general body meeting of NSSI has also been held. It has been attended by many members of NSSI. During the meeting, the second NSSI neutron newsletter dated November 2022 has been released.

Inauguration of NPCM-2022

Participants of NPCM-2022

S. M. Yusuf
Neutron Scattering Society of India

Highlights of Neutron Research

Experimental verification of phase separation mechanism in Fe-Cr alloy system: A combinatorial methodology combining APT and SANS

Identifying the operative mode of phase separation (spinodal decomposition (SD) or nucleation-growth (NG)) is key to the successful estimation of hardening of alloys that undergo phase separation under reactor environment. Since, the mechanical response of material to NG mode of phase separation is different from its response to SD; experimental verification of phase separation mechanism can help in selecting the appropriate mathematical models to estimate the mechanical response of phase separation reliably.

In this work, a correlative methodology combining atom probe tomography (APT) and small angle neutron scattering (SANS) techniques is adopted to analyze the Cr-rich ultrafine (spatial dimension < 10 nm) α' phase separation in ferritic Fe-Cr alloy system [1]. The framework first distinguishes the two different modes of α' phase separation by investigating two different series of thermally aged (773 K) Fe-35 at.% Cr and Fe-20 at.% Cr alloys. The methodology utilizes the output obtained from one technique for the analysis and meaningful interpretation of the data for the other. For example, independent APT analysis determines the mode of phase separation on the basis of: (i) presence / absence of periodic chemical fluctuation through radial distribution function analysis; and (ii) inter-phase interface characteristics (diffuse / sharp). SANS analysis, in contrast, yields virtually indistinguishable correlation peaks for both the modes, which necessitates further investigation of the several different aspects of SANS profiles in the light of the APT results. For the first time, key features of SANS profiles are identified that can unambiguously distinguish SD from NG in Fe-Cr system: (i) nature of temporal evolution of FWHM of the correlation peak; and (ii) appropriate value of γ for fitting with the dynamic scaling model ($\gamma = 6$ for SD, Fe-35 at.% Cr alloy; $\gamma = 4$ for NG, Fe-20 at.% Cr alloy). The process is demonstrated in details in Fig.1 below.

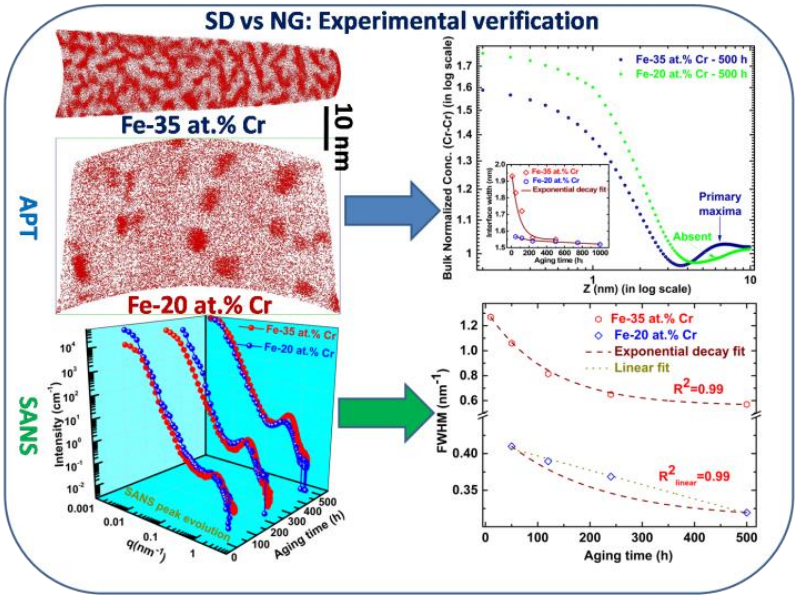

Fig.1: Experimental verification of phase separation mechanism using a combinatorial methodology combining APT and SANS. Each red dot represents one Cr-atom for APT.

1. *Nucleation-Growth Versus Spinodal Decomposition in Fe–Cr Alloys: An Experimental Verification by Atom Probe Tomography and Small Angle Neutron Scattering*; Sudip Kumar Sarkar, Debes Ray, Debasis Sen and Aniruddha Biswas, *Microscopy and Microanalysis* **29 (2)**, 437-450 (2023)

Contributed by Sudip Kumar Sarkar, BARC, Mumbai (email: sudip@barc.gov.in)

Effect of Pore Morphology on Opacity of Laser Host Ceramics

Neodymium doped Yttrium Aluminium Garnet (Nd: YAG) and Y_2O_3 (Nd: Y_2O_3) are well-known laser host materials for high-power laser applications. However, microstructural defects, such as pores can significantly affect the opacity of optical grade cubic ceramics. In order to understand the role of pore structure in determining the optical transparency of laser host ceramics, highly transparent (>75%) and nearly opaque ceramic pallets of Nd: YAG, Nd: Y_2O_3 [Fig. (c & d)] synthesized by both co-precipitation (COP) and solid-state reaction (SS) methods were investigated using SANS-I &II instruments at Dhruva reactor [1]. Fig. (a & b) shows experimental (solid points) and calculated (solid line) SANS profiles of YAG (NYG) and Y_2O_3 (NY) ceramics prepared by both methods. The data were analysed considering polydisperse spherical pores. The calculated profile fits well with experimental data. The pore volume distributions obtained from the fits are plotted in Fig. (c & d). It is clearly indicated that ceramic pallets of both compounds contain pores of size $\langle D \rangle$ ~120 nm-230 nm and 28-58 nm. The porosity values calculated from these curves revealed that pallets prepared by SS method are nearly 10 times more porous than those obtained from the COP method and hence are optically opaque. Further, the attenuation coefficients calculated using the parameters obtained from SANS fits for laser wavelengths λ=300 nm, 450 nm, 645 nm and 1000 nm are 22.2 cm^{-1}, 4.5 cm^{-1}, 0.87 cm^{-1}, 0.48 cm^{-1} for YAG and 34.8 cm^{-1}, 3.5 cm^{-1}, 1.20 cm^{-1}, 0.78 cm^{-1} for Y_2O_3 (COP) ceramics. These values are in close agreement the optical transmission results. Our study shows that SANS is an excellent technique to correlate pore structure and optical properties of technologically important laser host ceramics.

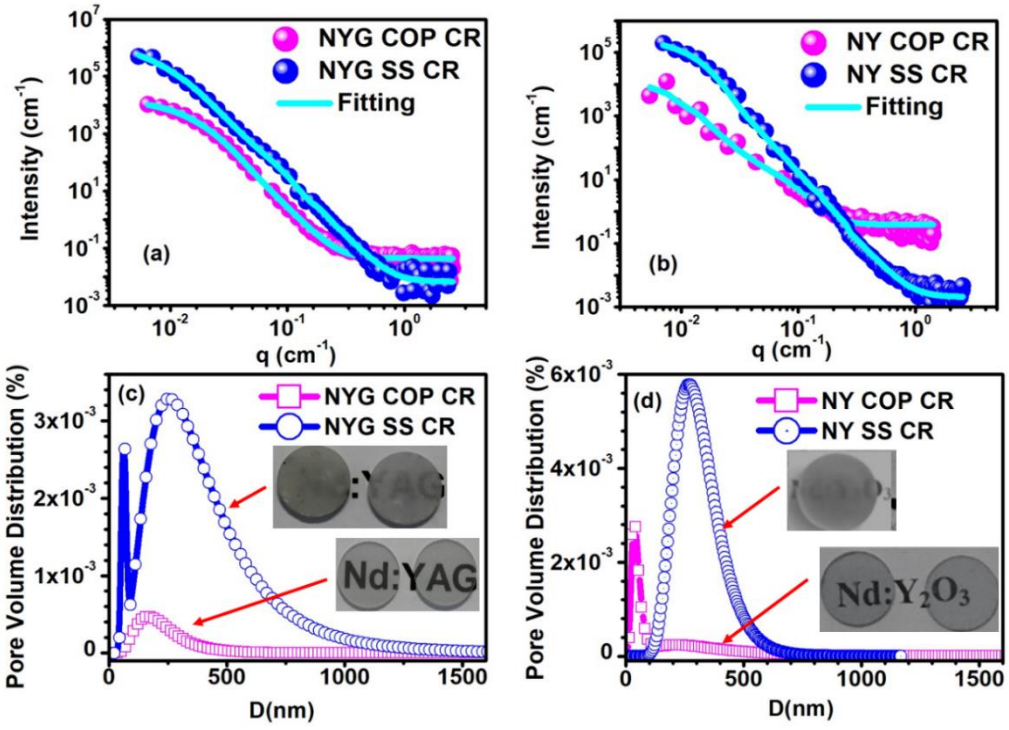

Figure. The SANS profile of (a) NYG-COP-CR and NYG-SS-CR and (b) NY-COP-CR and NY-SS-CR ceramic pellets. The solid line represents fitting to solid experimental points. Pore volume distribution of (c) NYG-COP-CR and NYG-SS-CR and (d) NY-COP-CR and NY-SS-CR ceramic pallets obtained from fitting of SANS profiles. Inset shows the photograph of respective ceramics.

1. *Effect of particle and pore morphology on optical transmission of yttria based laser host ceramics: A small-angle scattering investigation*, R. Selvamani, S. Kumar, G. Singh, D. Sen and P.U. Sastry, Nucl. Instrum. Methods Phys. Res. B **537**, 104 (2023).

Contributed by R. Selvamani, BARC, Mumbai (email: rachana@barc.gov.in)

Tuning Heat-Induced Protein Gelation by Controlling Inter-Protein Interactions

Globular proteins are known to undergo denaturation and eventually gelation on heating at temperatures more than their gelation temperatures. Heating of protein solutions gives rise to the denaturation of protein by disruption of the hydrogen as well as di-sulfide bonds, resulting into the exposure of internally directed hydrophobic sites. The instability of these sites indues a net hydrophobic attraction between unfolded protein chains leading to gelation by forming intermolecular network structure. However, the charges present on protein molecules tries to prevent such networking by invoking the electrostatic repulsion between them. It is therefore the counter-play of the attractive hydrophobic and repulsive electrotactic interactions which governed the fate of protein solutions on heating. The protein denaturation/gelation may be undesired, particularly in the cases where it leads to disruption of biological processes, however it may also be required for the applications related to food and biomedical industry.

In this work, we explored the pathways to control the temperature driven protein gelation by manipulating the electrostatic and hydrophobic interactions [1]. As both of these interactions can be simultaneously modified using ionic amphiphiles, we employed the complexation of protein with amphiphiles to tune the sol-gel transitions. Fig. 1a shows the gelation states of the pure BSA, and BSA in the presence of anionic sodium dodecyl sulfate (SDS) and non-ionic nonionic decaoxyethylene n−dodecylether (C12E10) surfactants. Anionic SDS prevents whereas nonionic C12E10 surfactant supports the protein gelation. The presence of SDS and C12E10 both, suppresses the SDS induced resistance against the protein gelation and the solution state of the BSA-SDS system undergoes gelation (Fig. 1a). Small-angle neutrons scattering (SANS) study (Fig. 1b) shows that SDS monomers binds to the oppositely charged sites of protein and thereby increasing the electrostatic repulsion between protein molecules to suppress the protein gelation. However, addition of C12E10 along with SDS leads to the preferential binding of SDS with C12E10 to form free mixed micelles, inducing the release of the SDS monomers from protein, and hence reverting the SDS-induced prevention of protein gelation. The BSA and BSA+SDS+C12E10 systems are found to be attractive while BSA+SDS system repulsive at temperatures near to their gelation temperatures (Fig. 1c). The present study shows how interprotein interactions can be modified to control the protein gelation or even other phases.

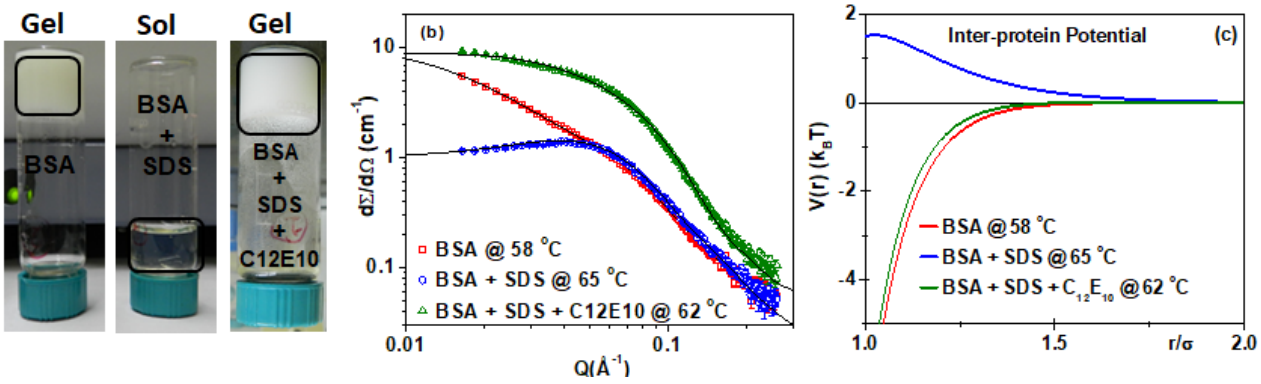

Fig. 1 (a) Physical states of protein-surfactant samples at 80 oC (above gelation temperatures). (b) SANS data of BSA, BSA+SDS and BSA+SDS+C12E10 systems at temperatures below, their respective gelation temperatures and (c) fitted corresponding potentials.

1. *Modifying interprotein interactions for controlling heat-induced protein gelation*, Sugam Kumar, D. Saha, V. K. Aswal, Phys. Rev. Mat. **7**, 015601 (2023).

Contributed by Sugam Kumar, BARC, Mumbai (email: sugam@barc.gov.in)

Coupled soft vibrations of Li and SiO_4 enable Li-ion diffusion in amorphous $Li_2Si_2O_5$

The future of solid-state batteries depends on the performance and thermodynamic stability of solid-electrolytes at ambient conditions. The design of new solid-electrolytes depends on the microscopic understanding of atomic diffusion processes and its correlations with structure and dynamics of the lattice. In this work, we demonstrated that the coupling of the Li dynamics with the dynamics of its neighboring SiO_4 polyhedral units in the amorphous phase of $Li_2Si_2O_5$ helps to accelerate the Li^+ diffusion [1]. Using neutron scattering experiments supplemented by ab-initio molecular dynamics (AIMD) simulations, we investigate the atomic dynamics and Li^+ diffusion in crystalline and amorphous $Li_2Si_2O_5$ (Figure 1). The neutron measurements in the amorphous phase of $Li_2Si_2O_5$ show the fast Li^+ diffusion and localized dynamics of SiO_4 units and presence of large phonon density of states at low energy (low-*E*) in the superionic amorphous phase. These low-*E* states disappear in the non-superionic crystalline phase, corroborating the role of low-*E* modes in Li^+ diffusion. These low-*E* modes involve a large amplitude of Li vibrations coupled with SiO_4 vibrations in the amorphous phase (Figure 2). At elevated temperatures, these vibrational dynamics help to accelerate the Li^+ diffusion. The insight gained in the structures and the dynamics from our studies will help to design better solid state batteries in the future.

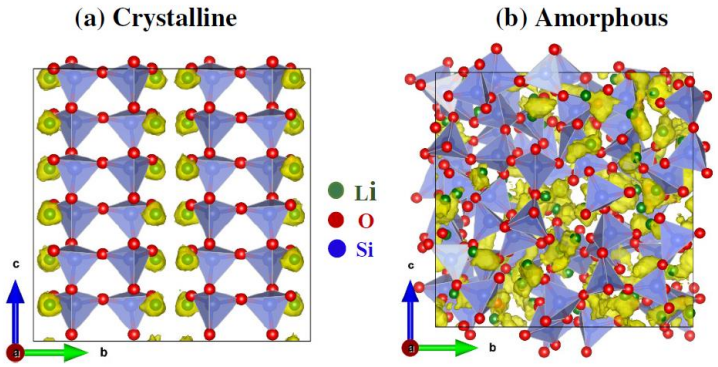

Figure 1. The structure of (a) *crystalline*- $Li_2Si_2O_5$ and (b) *amorphous*- $Li_2Si_2O_5$ used in simulations. The Li probability iso-surface plot (yellow dots) from AIMD simulations at 1000 K. The disjoint isosurface plots in crystalline- $Li_2Si_2O_5$ shows absence of Li^+ diffusion, while connected isosurface plots in amorphous phase reveal Li^+ diffusion.

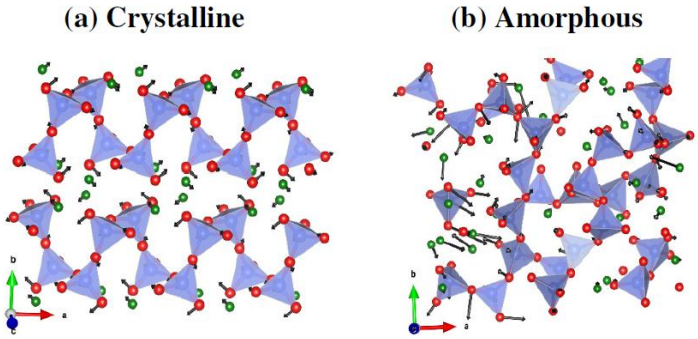

Figure 2. (a,b) The calculated eigenvector of 9.5 meV phonon in *crystalline*- $Li_2Si_2O_5$ and 4.5 meV phonon in *amorphous*- $Li_2Si_2O_5$. The enhanced amplitude of Li vibrations in the amorphous phase coupled with the surrounding SiO_4 dynamics accelerates the Li diffusion at elevated temperature.

1. *Soft anharmonic Li vibrations coupled with SiO_4 vibrations enable Li-ion diffusion in amorphous $Li_2Si_2O_5$*, Sajan Kumar, M. K. Gupta, P. Goel, R. Mittal, S. Mukhopadhyay, Manh Duc Le, R. Shukla, S. N. Achary, A. K. Tyagi and S. L. Chaplot, Journal of Mater. Chem. A **11**, 1712 (2023).

Contributed by R. Mittal, BARC, Mumbai (email: rmittal@barc.gov.in)

The Role of Crystal Structure on Ionic Conduction in Germanate Compound $A_2Cu_3Ge_4O_{12}$ (A = Na, K): A Neutron Diffraction Investigation

In modern society, rechargeable batteries play a significant role in energy storage and electronic gadget applications, with Li-based rechargeable batteries dominating the market.
However, due to the high cost, toxicity, and limited resources of lithium (which constitutes only ~0.002 wt % of Earth's crust), alternatives such as sodium (~2.36 wt % in Earth's crust) and potassium (~2.09 wt % in Earth's crust) ion-based compounds have gained special interest.
With this motivation, we have studied crystal structural and electrical properties of sodium and potassium based germanate compounds $A_2Cu_3Ge_4O_{12}$ (A = Na, K) by comprehensive neutron powder diffraction (NPD) and impedance spectroscopy studies [1]. We found that the crystal structures of $K_2Cu_3Ge_4O_{12}$ (KCGO) and $Na_2Cu_3Ge_4O_{12}$ (NCGO) compounds are made of perfect 2D and quasi-2D alkali metal ion layers, respectively. For both the compounds, we have determined that the ionic conductivity is due to small polaron hopping with activation energies 0.90(3) and 1.22(6) eV for KCGO and NCGO, respectively [Fig. (a)]. It is found that the value of K-ionic conductivity in KCGO is higher than the value of Na-ionic conductivity in NCGO, despite sodium being lighter in weight and smaller in size than potassium. By conducting soft-bond valence sum (BVS) analysis of room temperature NPD patterns, we determined the conduction pathways of sodium and potassium ions within the crystal structure. The results indicated 2D conduction pathways in KCGO, while, while NCGO exhibited 1D channel-like pathways [Fig. (b) and (c)] with higher concentration of bottlenecks for Na-ionic conduction. Such differences in the conduction pathways results in lower ionic conductivity and higher activation energy for NCGO as compared to KCGO. Moreover, we found that the constant value of activation energy over the kHz frequency range makes these materials suitable for potential applications in avalanche beacons, amateur, and geophysical sensors.

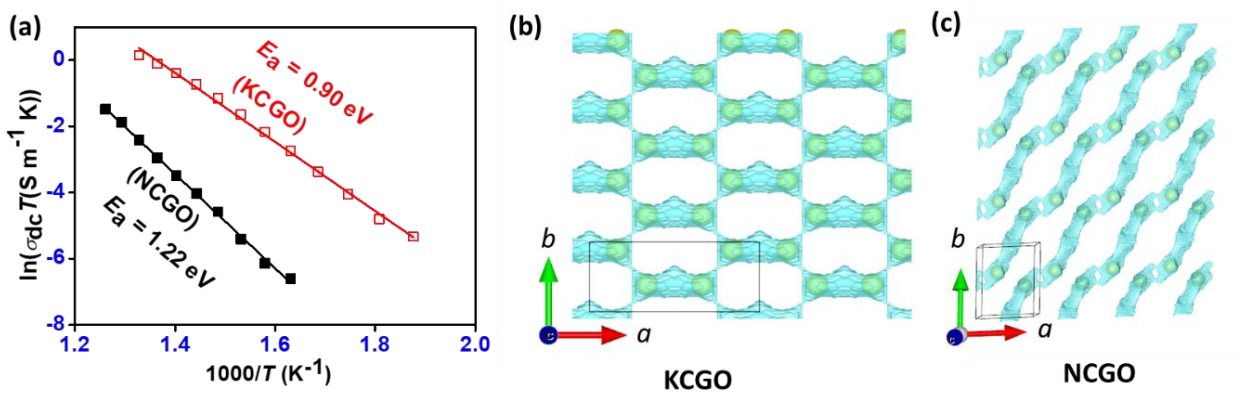

Figure: (a) Variation of $\ln(\sigma_{dc}T)$ as a function of inverse temperature for KCGO (open symbol) and NCGO (solid symbol) compounds. Solid lines are fitted curves by the small polaron hopping model. Ionic conduction pathways for (b) KCGO and (c) NCGO, respectively, determined from the soft-bond valence sum (BVS) analysis of room temperature NPD patters. The thin gray boxes show the dimension of the respective unit cell.

1. *Role of Crystal Structure on the Ionic Conduction and Electrical Properties of Germanate Compounds $A_2Cu_3Ge_4O_{12}$ (A= Na, K)*, K. S. Chikara, A. K. Bera, A. Kumar, S. M. Yusuf, ACS Applied Electronic Materials **5**, 2704-2717 (2023).

Contributed by A.K. Bera, BARC, Mumbai (email: akbera@barc.gov.in)

Two-dimensional short-range spin-spin correlations in the layered spin-3/2 maple leaf lattice antiferromagnet $Na_2Mn_3O_7$ with crystal stacking disorder

Geometrical frustration often induces a collective behaviour of the interacting spins. Especially, geometrically frustrated 2D spin systems based on triangular plaquettes reveal novel chiral spin correlations. 2D maple leaf lattice (MLL), formed by depletion of 1/7th lattice points from a regular triangular lattice, provides the possibility of multiple chiral spin states in comparison to a single chiral spin state in a triangular lattice. Here, we report the results of a comprehensive neutron diffraction study on $Na_2Mn_3O_7$ involving MLL of magnetic Mn^{4+} (spin-3/2) ions [1]. Room temperature neutron diffraction pattern [Fig. 1(a)] reveal the presence of both sharp and Broad Bragg peaks. Analysis of such pattern reveals the presence of stacking faults due to a sliding of $Mn_3O_7^{2-}$ layers [Fig. 1(b-c)]. The amount of such stacking faults has been successfully tuned by controlling the sample synthesis condition, i.e., annealing time. A reduction of the stacking faults has been found with increasing the annealing time during sample synthesis. Low temperature neutron diffraction study down to 5 K reveals an appearance of additional magnetic diffuse scattering [Fig. 1(d)]. Analysis of such diffuse magnetic scatterings using the Reverse Monte Carlo (RMC) method illustrates a 2D short-range antiferromagnetic (AFM) ordering in $Na_2Mn_3O_7$ with non-collinear spin arrangements. The 2D spin-spin correlations are evident from the rod like scatterings along the *l*-direction [Fig. 1(e-f)]. Our study further reveals that the spin-spin correlation length of the short-range AFM ordering enhances with the reduction of the intrinsic stacking faults i.e., with the increasing annealing time [Fig. 1(h)]. Our study highlights the role of underlying lattice geometry of 2D frustrated lattices having triangular plaquettes on the occurrence of novel chiral spin structures.

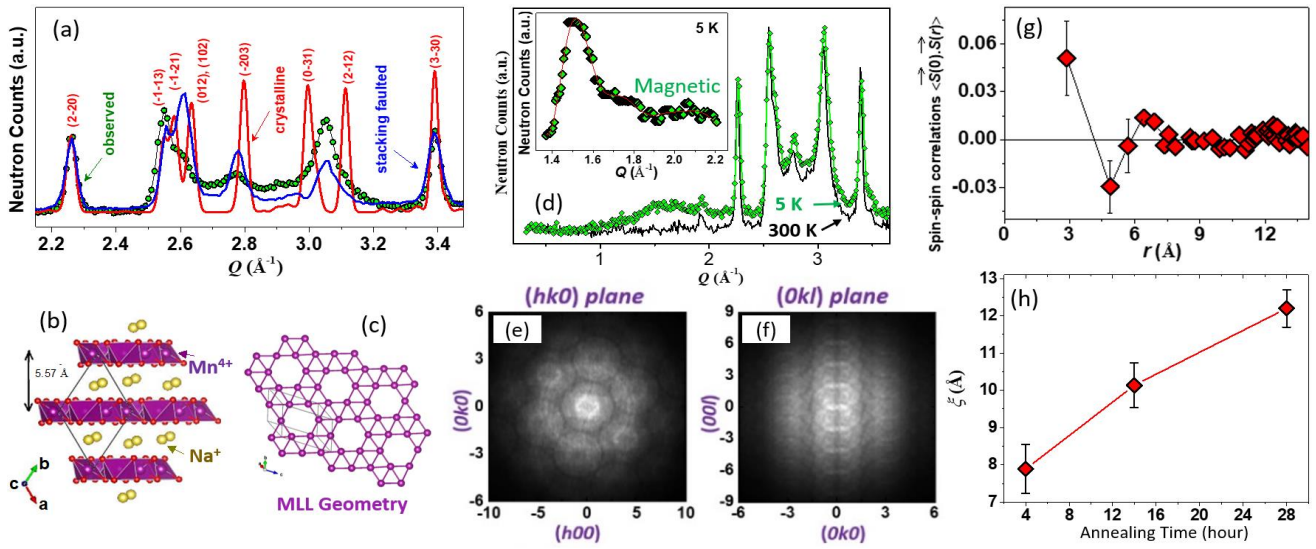

Figure. *(a) The observed (green) and simulated neutron diffraction patterns [by considering crystalline (red) and stacking faulted (blue) crystal structures] for $Na_2Mn_3O_7$. (b) The schematic layered crystal structure of $Na_2Mn_3O_7$. (c) The MLL geometry of Mn^{4+} ions. (c) Low temperature neutron diffraction pattern revealing diffuse magnetic scattering. Inset shows the comparison of the experimental pattern with the simulated pattern by RMC method. (e) and (f) The reconstructed diffuse magnetic scattering patterns for selective planes in the reciprocal space; revealing rod like scattering along the l-direction due to 2D short-range spin correlations. (g) The real-space spin-spin correlations as a function of distance, and (h) The annealing time dependent spin-spin correlation length (ξ) of the short-range AFM ordering.*

1. *Two-dimensional short-range spin-spin correlations in the layered spin-3/2 maple leaf lattice antiferromagnet $Na_2Mn_3O_7$ with crystal stacking disorder*, B. Saha, A. K. Bera, S. M. Yusuf and A. Hoser, Phys. Rev. B **107**, 064419 (2023).

Contributed by A.K. Bera, BARC, Mumbai (email: akbera@barc.gov.in)

Neutron investigations of negative magnetization and exchange-bias in $DyFe_5Al_7$

We have studied three-magnetic-sublattice-based $DyFe_5Al_7$ compound of the RFe_5Al_7 (R = rare-earth) family to explore the coexistence of technologically important phenomena of NM and EB [Figs. 1(*a*-*e*)] by employing neutron diffraction and neutron depolarization techniques [1]. A full compensation of magnetization of randomly oriented magnetic domains (at the T_{COMP}) in the sample is clearly demonstrated by employing mesoscopic neutron depolarization technique [Fig. 1(b)]. Neutron diffraction study has revealed the asymmetric thermal variations of ferrimagnetically coupled Dy and total Fe magnetic moments leading to a sign change of net magnetic moment at the T_{COMP} [Fig. 1 (c)]. We report exchange-bias, for the first time, below the T_{COMP} in the compound [Fig. 1(e)] that shows an anomalous behaviour due the presence of field-induced spin reorientation. Our study has revealed a microscopic understanding of negative magnetization in this three magnetic sublattice system, and provided correlations among exchange-bias, magnetic compensation, and spin-reorientation phenomena.

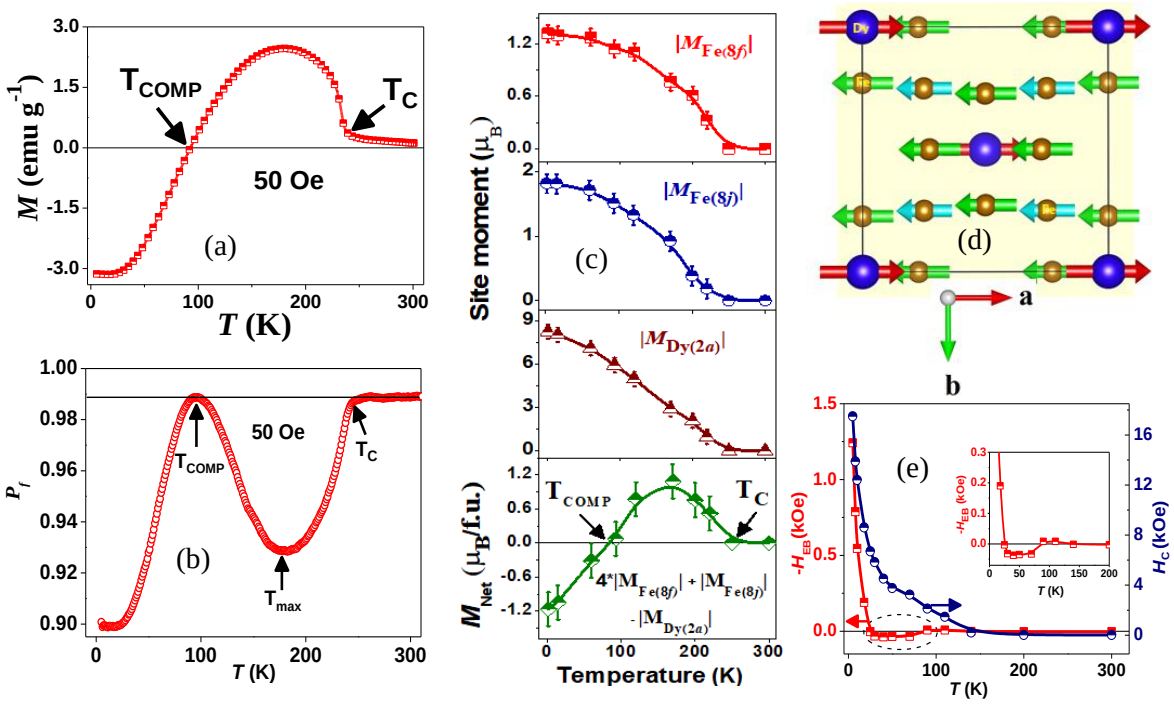

Fig.1(a) The observed negative magnetization in experimental dc magnetization data of $DyFe_5Al_7$. (b) Neutron depolarization curve showing zero domain magnetization at the compensation temperature (T_{COMP}). (c) Thermal variations of sublattice moments. (d) Magnetic unit cell at 1.5 K. (e) Variations of exchange-bias (H_{EB}) and coercivity (H_C) as a function of temperature.

1. *Insight into the negative magnetization and anomalous exchange-bias in DyFe5Al7 through neutron depolarization and neutron diffraction studies*, Deepak, Amit Kumar, S. M. Yusuf and E. V. Sampathkumaran, J. Phys.: Condens. Matter **35** 065802 (2023).

Contributed by Amit Kumar, BARC, Mumbai (email: amitkr@barc.gov.in)

Role of neutron diffraction in identification of phase displaying converse and direct magnetoelectric effect in double perovskite $LaYFe_2O_6$

Several oxide based materials are being studied for exhibiting intriguing properties, Magnetoelectric (ME) materials are one of the class in these materials. These properties have potential application in fundamental and applied physics, which can steer the demand in the various areas of modern civilization such as in sensors, spintronics, multi-state memory devices, long-searched electric-writing magnetic-reading random access memory, etc. Among magnetoelectric materials converse ME (CME) effect is defined as tuning of magnetic order parameter upon application of electric field, whereas electric polarization can be tailored by magnetic field in the direct ME (DME) effect. The CME effect can be employed in electric field tuneable devices, ME-RAMs, and spintronics; the working of magnetic sensors, transformers, and energy harvesters is based on the DME. Concomitant occurrence of these two effects is very worthwhile in the development of various innovative technological promises.

Among several compound under research for showing these properties, double perovskite based $LaYFe_2O_6$ is being studied which exhibit biphasic symmetry which is consisting predominantly in Pbnm space group and minorly in P21nm space group. Though it was found that $P2_1nm$ have potential of ME effect. Here in this report the samples prepared by modified sol-gel preparation method and sample in $P2_1nm$ space group was found to be in majority phase.

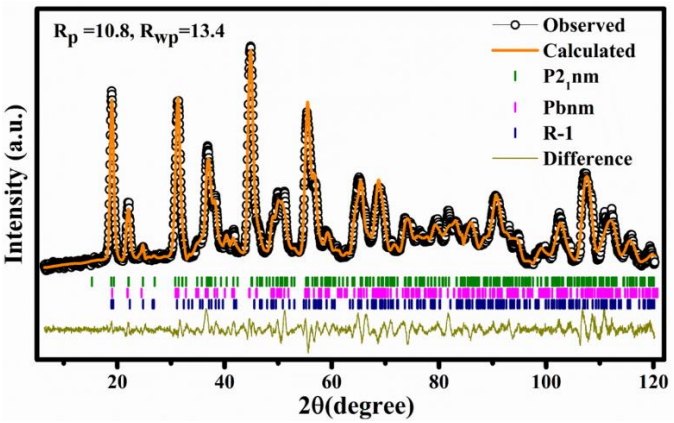

Fig: Rietveld refined neutron powder diffraction pattern of $LaYFe_2O_6$ sample at RT. R-1 Bragg positions are due to the contribution from the magnetic phase of $P2_1nm$ symmetry.

XRD confirmed best crystallinity which was further investigated via neutron powder diffraction (ND) measurement at powder diffractometer (PD-3) at 1.48 ^{0}A wavelength. Figure show the Rietveld refined room temperature ND pattern. Here, both the crystallographic phases ($P2_1nm$ and Pbnm) are considered for the refinement. It is observed that the presence of Pbnm symmetry is very less in the material and hence magnetic contribution from $P2_1nm$ phase only are included in the refinement.

The refinement of magnetic phase is done by R-1 space group with symmetry operators of basis functions of irreducible representations and is calculated by BasIreps program using propagation vector k = (0,0,0). Lower values of reliability factors related to goodness of fit suggests a good agreement between observed and theoretically predicted one. ND refinement also indicate the alternate ordering of La and Y ions [~ 88.61(1) % of $P2_1nm$ phase] as well as suggests antiferromagnetic arrangements of the Fe spins at room temperature and the magnetic moment so obtained is 5.90 μ_B for Fe^{3+} [1]. Other characterization such as magnetization, M-E study, SEM etc have confirmed the converse magnetoelectric properties in the compound.

1. *Display of converse and direct magnetoelectric effect in double perovskite LaYFe2O6*, R. Ghosh, A. Barik, M. R. Sahoo, S. Tiwary, P. D. Babu, S. D. Kaushik, P. N. Vishwakarma, Journal of Applied Physics **132**, 224107 (2022)

Contributed by S.D. Kaushik, UGC-DAE CSR, Mumbai (email: sdkaushik@csr.res.in)

Multiferroicity in Haldane-spin chain Compound Tb_2BaNiO_5: Role of Critical Canting Angle

Tb_2BaNiO_5 is a well-known exotic multiferroic system, exhibiting two antiferromagnetic anomalies at T_{N1} = 63 K and T_{N2} = 25 K, where the ferroelectricity appears below T_{N2} only. Among other rare-earth (*R*) systems of the stoichiometric formula, R_2BaNiO_5, the Tb compound is known to exhibit highest magnetodielectric (MDE) coupling of 18%. The nuclear (crystallographic) space group of Tb_2BaNiO_5 is *Immm*, which is non-centrosymmetric and low temperature synchrotron and neutron diffraction studies show that the crystalline symmetry does not change as the system is cooled down to lowest temperature across its antiferromagnetic temperatures. The magnetic space group at the onset of the magnetic ordering, T_{N1} is found to be *Cm'*, which is a non-centrosymmetric, polar space group allowing polarization along *x* and *z* direction. The magnetic symmetry does not change across T_{N1} or T_{N2} and remains same till the lowest temperature. It is also to be noted that ferroelectricity does not set in at 63 K, but at 25 K, thus exhibiting the magnetodielectric coupling in this compound below 25 K [1].

It is interesting to note that below 25 K, the critical canting angle ($\Delta\theta$), i.e., the difference between the angles Tb (θ_{Tb}) and Ni (θ_{Ni}) spins makes with respect to *c*-axis, crosses a certain threshold and increases sharply as temperature is decreased further. This observation has been tested in compounds exhibiting and losing MDE on subjecting to internal (chemical substitutions) and external (pressure, magnetic field) perturbations. The magnetic ordering temperatures (T_{N1}, T_{N2}) are influenced by these perturbations, however, in every case it has been observed that the system exhibits MDE only when $\Delta\theta$ *crosses a certain threshold* at T_{N2} of that system. We therefore infer that the critical canting angle is made up of two components – cooperative (long-range) and local (short-range) contributions and is dependent upon the system being studied.

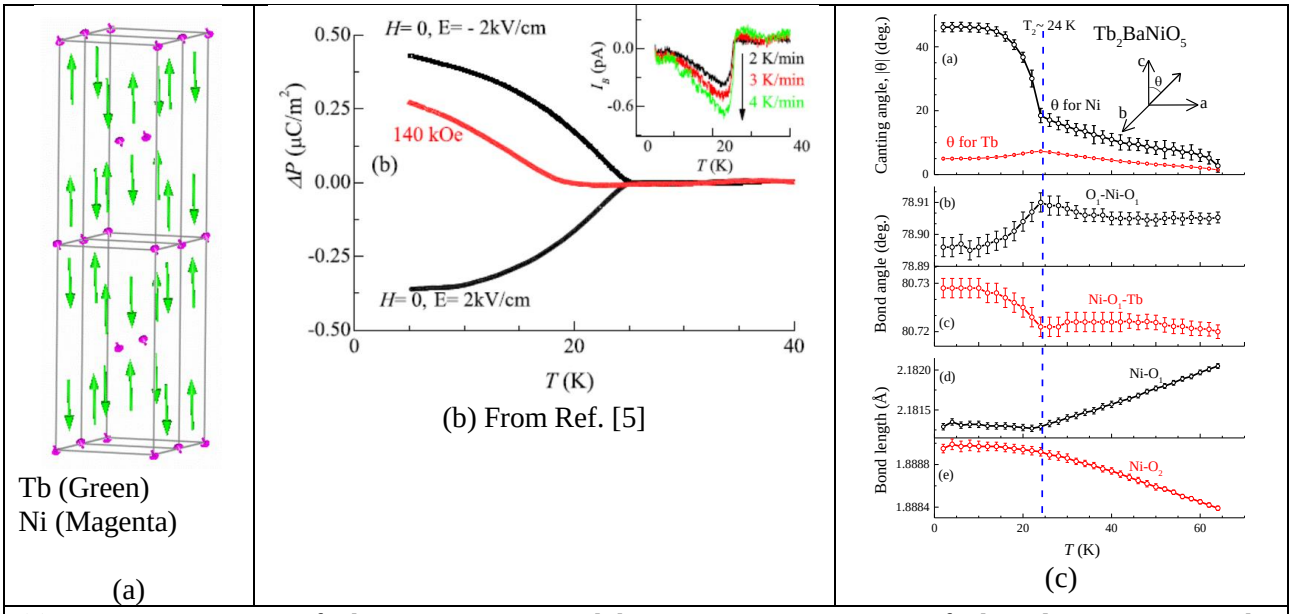

(a) Magnetic structure of Tb_2BaNiO_5 at 2K, exhibiting spin arrangements of Tb and Ni moments. The canting of Tb (θ_{Tb}, green) and Ni (θ_{Ni}, Magenta) spins with respect to c-axis is clearly visible. (b & c) The plot of polarization (as ΔP) and the critical canting angle ($\Delta\theta = |\theta_{Tb} - \theta_{Ni}|$) is plotted as a function of temperature and other structural parameters, respectively. The sharp increase in $\Delta\theta$ below the 25K is clear, which confirms the role of critical canting angle in inducing multiferroic properties in Tb_2BaNiO_5.

1. *Canting Angle Behavior of Magnetic Moments in Y-Substituted Tb2BaNiO5 and Its Relevance for Magnetoelectric Coupling*, Ram Kumar, S. Rayaprol, A. Hoser and E.V. Sampathkumaran., Phys. Status Solidi B, 2300042 (2023)

Contributed by S. Rayaprol, UGC-DAE CSER, Mumbai (email: sudhindra@csr.res.in)

Melting long-range magnetic order in metallic Tb_5Si_3 by magnetic field: Similarities with Kitaev insulators

Quantum spin liquid (QSL) is generally characterized by its long-range quantum entanglement, fractionalized excitations and absence of ordinary magnetic order. Kitaev materials, having honeycomb network of magnetic ions are promising cases for QSL. Experimentally, several Kitaev materials have been synthesized, which includes the honeycomb materials, Na_2IrO_3, α-Li_2IrO_3, $H_3LiIr_2O_6$, α-$RuCl_3$ etc. In these insulating materials which order magnetically, the Kitaev spin-liquid state has been claimed to be achieved by suppressing the stronger non-Kitaev spin exchange channels, responsible for magnetic ordering, by a sufficiently strong magnetic field, H. The disappearance of magnetic ordering features in bulk measurements such as magnetic susceptibility (χ) heat-capacity (C) at a critical field (H_{cr}) has been considered as a key indicator of Kitaev physics.

The rare-earth system containing honey-comb network of Tb ions, Tb_5Si_3 exhibits suppression of long-range magnetic order (T_N = 69 K) at H_{cr} in heat capacity and magnetization data, mimicking the behavior of Kitaev physics materials. Neutron diffraction experiments on polycrystalline sample of Tb_5Si_3, as a function of temperature and magnetic fields, reveal that it is an incommensurate magnetic structure that gets suppressed, showing peaks arising from multiple wave vectors beyond H_{cr} [1].

The experimental work carried out by us brings out a parallel with the field-dependence of the bulk properties of QSL candidates, which turned out to fall under the category of '***promising Kitaev spin-liquids***'. The main departure from the usual Kitaev spin-liquid systems and present work is that Kitaev physics is usually discussed in non-metallic systems, where as Tb_5Si_3 is metallic, thus stating the fact that the understanding of Kitaev materials is still incomplete. Recently, there are several theoretical attempts extending Kitaev honeycomb model to a generalized higher spin emphasizing the need to consider various other interactions. We therefore propose that it is of interest to explore whether bond-dependent interactions arise leading to Kitaev-like physics within RKKY interaction.

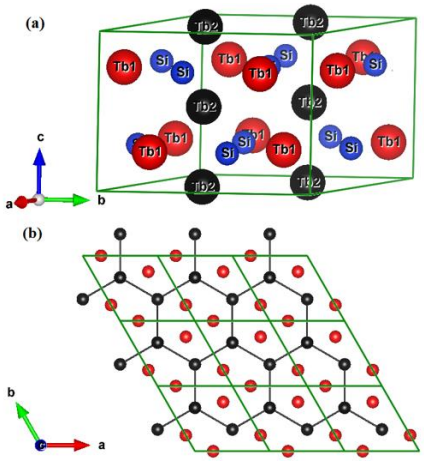

Crystal structure of Tb_5Si_3. (a) Unit cell, and (b) Tb2 honeycomb layer along with adjacent Tb1 layer (omitting Si). The green line represents unit-cell boundary

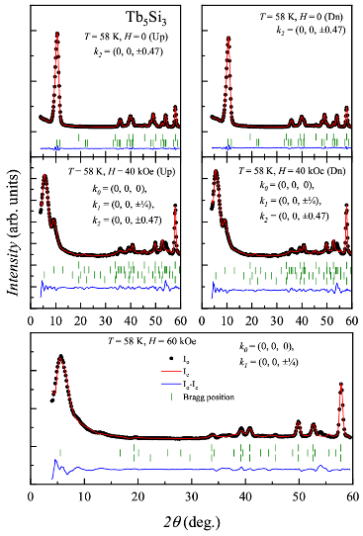

Rietveld refinement of ND patterns recorded for T = 58 K, which is just below T_N ~ 69 K, in the presence of applied magnetic fields up to H = 60 kOe. Different magnetic structures corresponding to multiple propagation vectors were used to refine the magnetic structures at different applied fields. With increasing field, commensurate magnetic phase dominates at the expense of the incommensurate phase.

1. *Magnetic-field induced melting of long-range magnetic order akin to Kitaev insulators in the metallic compound Tb5Si3*, S.Rayaprol, K.K. Iyer, A. Hoser, M. Reehuis, A.V. Morozkin, V. Siruguri, K. Maiti and E.V. Sampathkumaran, J. Phys.:Condens. Matter **35**, 305801 (2023)

Contributed by S. Rayaprol, UGC-DAE CSER, Mumbai (email: sudhindra@csr.res.in)

Interface morphology driven exchange interaction and magnetization reversal in the Gd/Co multilayer

Rare-earth (RE)/transition metal (TM) ferromagnetic heterostructures with competing interfacial coupling and Zeeman energy provide a rich ground to study different phase states as a function of magnetic field and temperature. Interface morphology as a knob in these RE/TM heterostructures provides an excellent opportunity to engineer the macroscopic magnetic response by tuning the interface dependent microscopic interactions between the layers. We have investigated the interface morphology driven structure and magnetic properties of Gd/Co multilayer. The interface morphology of the multilayer was controlled by annealing the multilayer at a relatively low temperature of 573 K under a vacuum condition. Combining the different experimental techniques and a simple one-dimensional spin-based model calculation, we studied the detailed magnetic structure and magnetization reversal mechanism in this system across compensation temperature (T_{cmop}), which suggested a strong interface dependent coupling in the system [1]. We showed that changes in interface morphology of the Gd/Co multilayer strongly influence the macroscopic magnetic properties of the system. The calculation also confirms the formation of a helical magnetic structure with a 2π domain wall in this system below T_{cmop}. The experimental finding and the simulation of this technologically important system will help to understand the physics of all-optical switching and related applications. Figure 1 (a) show the Schematic representation of Gd/Co bilayer before and after annealing at 573 K. On annealing we observed alloy formation at interfaces which modify the antiferromagnetic exchange interaction and thus show different macroscopic magnetization (Fig. 1(b)) response (different T_{cmop} and splitting in ZFC/FC data). Different magnetic depth profiles across the interface were obtained from PNR data at room temperature (Fig. 1(c)). Using a simple spin model, we explained a detailed view of the micromagnetic structure that is responsible for the modification in magnetization. Spin model analysis suggested interface induced AFM exchange interaction provided a different magnetic structure as a function of field and temperature.

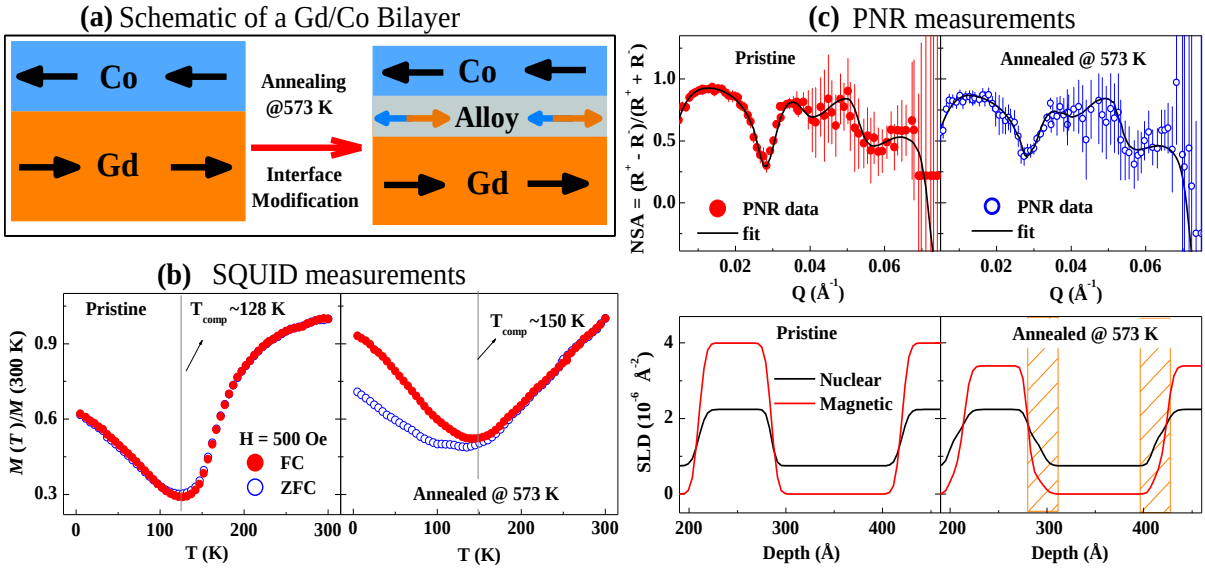

Figure 1: (a) Schematic representation of Gd/Co bilayer before and after annealing. The opposite sign of the arrow suggests strong antiferromagnetic coupling in the Gd and Co layers. (b) Magnetization data for ZFC and FC conditions as a function of temperature from pristine and annealed multilayer at 573 K. (c) PNR data represented as normalized spin asymmetry (NSA) from pristine and annealed multilayer. Lower panel represent the nuclear and magnetic depth profile across interfaces of a Gd/Co bilayer.

1. *Interface morphology driven exchange interaction and magnetization reversal in a Gd/Co multilayer*, S. Singh, M.A. Basha, H. Bhatt, Y. Kumar and M Gupta, Physical Chemistry Chemical Physics **24**, 6580 (2022)

Contributed by S. Singh, BARC, Mumbai (email: surendra@barc.gov.in)

A short status review on a Neutron Technique

Single-crystal Neutron Diffraction at Dhruva: A tool to unravel the crystalline structure at atomic scale

R. Chitra and Rajul Ranjan Choudhury

Solid State Physics Division, Bhabha Atomic Research Centre, Mumbai 400085 India

rchitra@barc.gov.in, rajul@barc.gov.in

Abstract

Diffraction of monochromatic beam of neutrons having wavelength of the order of magnitude of interatomic distances in crystalline solids can reveal atomic structure of the crystal at unit cell level. This information is very important not only for understanding the fundamental properties of the crystalline solids but also for tailoring these properties for various technological applications. The main advantage of single crystal neutron diffraction over its complementary technique of single crystal X-ray diffraction is that it can provide the atomic positions of lighter elements like Hydrogen, Lithium etc to the same accuracy as the positions of heavier elements like Iron, Lead etc present within a unit cell. Because of this unique advantage, single crystal neutron diffraction is a technique used mainly to study the structure of crystals where hydrogen bonding plays an important role in determining the crystal properties. This review gives a brief overview of the single crystal neutron diffraction studies conducted at the Dhruva and CIRUS reactors located in Trombay, Mumbai.

1 Introduction

In order to understand the properties of condensed matter (crystalline or amorphous solids, and liquids) one requires a detailed knowledge of the positions as well as the movements of its constituent atoms. Scattering of radiation is one of the most effective experimental means of acquiring such information. When the radiation passes through matter, it is scattered by its constituent atoms with a certain probability (scattering amplitude), without (elastic scattering) or with (inelastic scattering) change in energy [1]. As the incident radiation having wavelength of the order of magnitude of the interatomic distances meets an assembly of ordered atoms in a crystalline solids it gets scattered in all directions, the wave scattered by the different atoms may have a phase relationship and interfere (coherent scattering, with summation of amplitudes) resulting in a diffraction pattern, or they may have random phases (incoherent scattering, with summation of intensities) resulting in uniform background radiation. The angular distribution of the coherent elastic scattering can provide information on the spacing of the atoms; the relative intensities in different directions reflect the chemical structure.

Single crystal diffraction is a non-destructive analytical technique that provides the detailed information including unit cell dimensions, crystal space group symmetry, atomic vibrations and atomic positions within a unit cell, bond lengths, bond angles etc about crystalline solids [2]. As the name suggests the samples studied by this experimental technique are single crystals characterized by an orderly three-dimensional arrangement of atoms, ions or molecules that is repeated throughout the entire sample volume i.e. the crystal lattice is continuous and unbroken in the entire sample.

Ordinarily when such a sample is illuminated with monochromatic radiation for a generic crystal orientation, no coherent elastic scattering is observed, only for certain crystal orientations when a particular set of crystalline plane satisfy the Bragg's condition shown in figure-1 that one detects coherent elastic scattering intensity

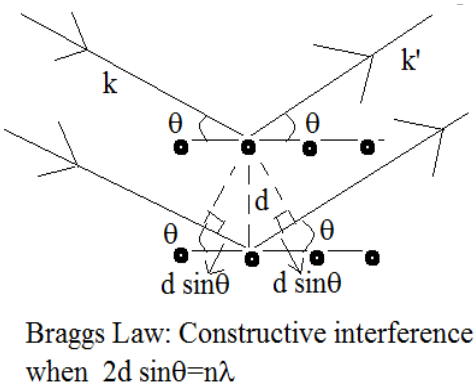

Figure 1. A schematic of Bragg scattering from a pair of atomic planes

In general, the experimental apparatus used to perform diffraction experiment on single crystals should have three essential components i) Radiation source ii) sample stage which enables the sample to be oriented and iii) a radiation detector.

This status review aims to give a glimpse of single crystal neutron diffraction studies conducted at Dhruva and Cirus reactor located in Trombay Mumbai. First of all, the basic principles of single crystal diffraction are discussed briefly to give an overview of how structure solution using diffraction data proceeds. This is followed by details of the 4-circle single-crystal diffractometer and importance of using neutron radiation for diffraction studies. Finally examples of studies conducted at the above-mentioned diffractometer are discussed to give the flavour of the technique.

2 Basic principles of crystal structure solution

Solid state of matter is characterised by close packing of its constituent particles which can be neutral atoms, ions or molecules so as to ensure that the solid objects have specific shape, mass, and volume. Based on the arrangement of the constituent particles there can be two type of solids, amorphous and crystalline solids, former having only short range local ordered arrangement of its constituent particles, whereas latter is characterised by long range ordered arrangement of its constituent particles resulting from infinite repetition in space of identical structural units [1]. Hence the structure of all crystalline solid can be described by a lattice describing the translational order in three-dimensional space and structural units called the basis that are attached to each of the lattice points so as to reproduce the entire crystalline volume. Thus,

Crystal=Lattice + Basis

Lattice is defined by three fundamental translation vectors **a**, **b**, **c** such that arrangement of constituent particles looks the same in every respect when viewed from two points **r** and **r'** related to each other as following:

r'=**r**+**T** where **T** = u**a**+v**b**+w**c** : u, v, w are arbitrary integers

Here, **T** is called the lattice translation operation and parallelepiped volume encloses by the three fundamental vectors **a**, **b**, **c** is called unit cell.

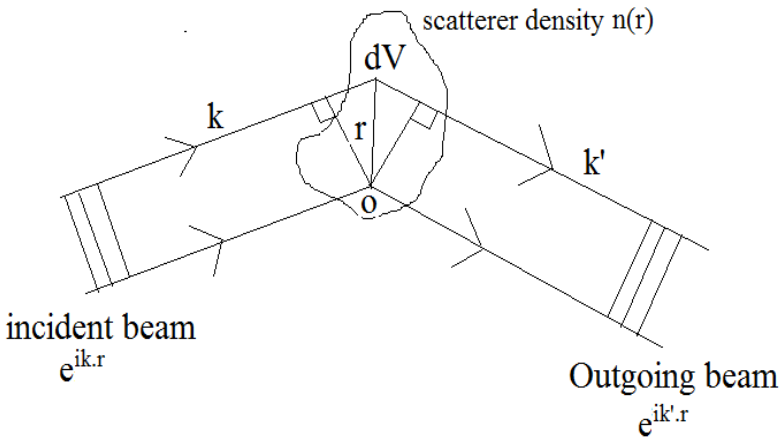

Figure 2. General scattering of incident beam of radiation $e^{ik.r}$ by a scatterer density n(r).

2.1 Structure Factor

All the physical properties of crystals including its atomic density ρ(r) at a given point r within a unit cell is invariant under lattice translation operation **T**:

$\rho(\mathbf{r}) = \rho(\mathbf{r}+\mathbf{T})$

This is a direct consequence of the way crystals are defined. Since ρ(r) is a periodic function for crystalline solids, one can represent it by Fourier representation as following:

$\rho(r) = \sum_G \rho_G e^{iG.r}$ Where G=h**a***+k**b***+l**c*** ; h ,k, l are integers

ρ_G are the Fourier coefficients and **G** wavevectors of plane waves in the Fourier series as defined above are called the reciprocal lattice vectors. The complete set of G vectors gives us the reciprocal lattice which has the following relationship with the direct crystalline lattice.

a.**a***=2π, **a**.**b***=0, **a**.**c***=0

a.**b***=0, **b**.**b***=2π, **b**.**c***=0

a.**c***=0, **b**.**c***=0, **c**.**c***=2π

The reciprocal lattice plays a fundamental role in the theory of diffraction; the momentum difference between incoming and diffracted beam from a crystal is a reciprocal lattice vector, as a result the diffraction pattern of a crystal can be used to determine the reciprocal vectors of the lattice. When an incident beam of radiation ($e^{ik.r}$) is diffracted from a scatterer density ρ(r) resulting in a diffracted beam ($e^{ik'.r}$) (Figure-2), one can obtain the total amplitude A of diffraction in **k'** direction as following:

$$A = \int dV\rho(r)\exp[i(k-k').r] = \sum_G \int dV\rho_G \exp[i(G-\Delta k).r]$$

When Δk differs significantly from G, A is negligibly small but when G = Δk the argument of the exponential vanishes we get for crystal with N unit cells

$A = N \int dV_{cell}\rho_{uc} \exp(-iG.r) = NF_G,$

The quantity F_G is called the structure factor and is defined as an integral over single unit cell with r=0 at one corner. If unit cell contains S atoms and r_j is the vector to the centre of the jth atom, then one can write unit cell scatterer density $\rho_{uc}(r)$ as a superposition of atomic concentration function n_j associated with each atom j of the cell

$\rho_{uc}(r) = \sum_{j=1}^{s} n_j\,(r - r_j)$

Hence the structure factor can be written as integral over S atoms of a cell

$$F_G = \sum_{j=1}^{s} \int dV_{cell}\, n_j(r - r_j) \exp(-iG.r) = \sum_{j=1}^{s} f_j \exp(-iG.r_j)$$

Since: $G.r_j = 2\pi(kx_j+ky_j+lz_j)$

$$F_{hkl} = \sum_{j=1}^{s} f_j \exp\left[-2\pi i\left(hx_j + ky_j + lz_j\right)\right] = |F_{hkl}|e^{i\varphi hkl}$$

Here, f_j is the atomic form factor and it gives a measure of the scattering power of the jth atom of the unit cell. One can see from the description above that structure factor in general is a complex quantity i.e. it has amplitude $|F_{hkl}|$ as well as a phase ϕ_{hkl}. At any given finite temperature of the crystals the constituent atoms are never at rest, vibration of the jth atom by a small amount u about its equilibrium position r_j results in the smearing of the atomic density and this has a direct consequence on the diffraction intensities, the structure factor gets modified due to these vibrations as following:

$$F_G = \sum_{j=1}^{s} f_j \exp(-iG.r_j)\langle\exp(-iGu_j)\rangle$$

Here, F_G is called the thermal average structure Factor. Structure factor is proportional to the Fourier transform of the scatterer density integrated over unit cell hence if we can obtain a complete set of F_G we can get the unit cell scatterer density ρ(x, y, z) which is the final aim of all structure solution experiments

$$\rho(x,y,z) = \frac{1}{V}\sum_{hkl} |F_{hkl}| \exp(-2\pi i(hx + ky + lz - \varphi hkl)$$

2.2 Diffraction intensities

If the interaction of the incident beam of particle (photos/neutrons) with the matter is small then it is reasonable to assume that the incident particles are scattered only once within the entire crystal volume and the amplitude incident on every scattering centre inside the crystal is the same and multiple scattering within the crystal volume can be completely ignored, in such a case the total diffracted amplitude is simply obtained by adding the individual amplitudes scattered by each scattering centre. The resultant distribution of diffracted amplitudes in reciprocal space is the Fourier transform of the distribution of diffracting centres in physical space as described in the previous section, this theory of diffraction is called the "Kinematical theory of diffraction", the integrated diffracted intensities according to this theory are proportional to the square of the structure factor and to the volume of crystal bathed in the incident beam.

$$I_{hkl} \alpha F_{hkl}^2$$

In general for large perfect crystals the assumption that multiple scattering can be completely ignored is not true when such crystal is bathed with the incident beam of particle they are subject to multiple diffraction throughout the crystal; all of these waves can then interfere with each other resulting in net intensity which is less than that proposed by the Kinematical theory of diffraction. Theory describing the scattering of incident beam of particles from a large perfect crystal is more rigorous it

takes into account the interactions of the scattered radiation with matter; this theory is called the dynamic theory of diffraction. In the full dynamic limit, the integrated Bragg intensity is independent of the structure factor, and is instead proportional to the Darwin width, hence diffraction intensities from such perfect crystals cannot be utilized for structure solution. In order to get diffraction intensities that can be directly used to get the crystal structure, the sample crystal should be an ideally imperfect crystal consisting of slightly mis-oriented "mosaic" blocks, kinetic theory of diffraction gives a good description of diffraction intensities from such an ideally imperfect crystals, Integrated intensity of an (h,k,l) reflection from such a crystals is given as following

$$I_{hkl} = I^0 K (Lp/A)(F_{hkl}/V)^2$$

Where I^0 is the incident intensity, K is constant dependent on crystal size etc, L is the lorentz correction to the intensity (accounts for time required for a Bragg reflection to cross the surface of the sphere of reflection), p is polarization correction to the intensity (correction due polarization of the incident X-ray beam), A is the absorption correction (intensity of measured reflections is reduced by the absorption of X-rays/neutrons by the crystal), V is the unit cell volume and finally F_{hkl} is the structure factor.

2.3 Phase problem in crystallography

The radiation detectors used to obtain the diffraction patterns to record the diffraction intensity for each (h,k,l) reflection, since the individual diffraction intensity I_{hkl} for each of (h,k,l) reflections is proportional to the square of their structure factor ($|F_{hkl}|^2$), the phase information (ϕ_{hkl}) of these structure factor is lost. The problem of generating the phase information from the complete set of recorded diffraction intensities is called the phase problem in crystallography [3]. In unit cells of crystals of small and medium sized molecules (having molecular weight less than 1000Dalton) the atoms are normally well ordered, as a result diffraction intensities are measured to very high diffraction angles, in such cases the missing phase information is reconstructed directly from mathematical relationships between the phases of structure factors, this methods of solving the phase problem is are referred to as 'Direct Method'[4]. Two important properties of unit cell atomic densities that have been utilized to derive these mathematical relations are i) Atomicity: scatterer density within a unit cell is clumped into distinct atomic peaks, ii) Positivity: Scatterer density within a unit cell is positive throughout. The most important phase relationship called the triplet phase relationship between the phases of three strong reflection G(h_1, k_1, l_1), H(h_2,k_2,l_2) and -G-H(h_3,k_3,l_3) is given as following:

$$\varphi_H + \varphi_G + \varphi_{-H-G} \approx 0$$

if the two phases ϕ_G and ϕ_H can be guessed then the third phase $\phi_{\text{-G-H}}$ can be calculated using the triplet phase relationship. Hence starting from a small set of guessed phases a complete set of phases for strong reflections can be generated, resulting in a set of completely known structure factors, its Fourier transform can give the first approximation of the required scatterer density within a unit cell. These phase relationships become weaker as the number of atoms in the structure increases, as a result Direct Method cannot be used in large molecule crystallography. Some of the methods used to solve the phase problem in macromolecular crystallography are: Multiple Isomorphous Replacement method, Multiwavelength Anomalous Dispersion method, Molecular Replacement method etc.

2.4 Crystal Structure refinement

The initial structure obtained after solving the phase problem has to be refined to get atomic positions and atomic vibration parameters up to a required accuracy; one is reasonably close to the solution at this stage with only a few free parameters left to be determined. Structure refinement proceeds by minimising the difference between squared observed structure factors $|F_{obs}|^2$ and $|F_{cal}|^2$ calculated as a function of the free parameters [4]. Agreement between the observed and calculated structures is evaluated on the basis of the value of R-factor (reliability factor) defined as following:

$$R = \sum \frac{|F_{obs} - F_{cal}|}{|F_{obs}|}$$

The refinement is considered to be finished when the following essential conditions are fulfilled:

- R-factor is small enough.
- The structural model is chemically appropriate
- The estimated standard deviations of all geometrical parameters are as small as possible
- The peaks remaining in the difference Fourier map are as small as possible

3 Four-circle single-crystal diffractometer

In case of single-crystal diffraction experiments with monochromatic radiation, the most important instrumental criterion is to obtain the maximum flexibility in orienting the crystal, one way to accomplish this is to mount the crystal on an Eulerian cradle [2] having four concentric circles namely χ, ϕ, ω and 2θ (figure-3), including the detector arm, is known as a four-circle diffractometer. With a four-circle diffractometer, one can in principle (barring mechanical collisions and shadowing effects) access all nodes of the reciprocal space that are accessible for a given wavelength.

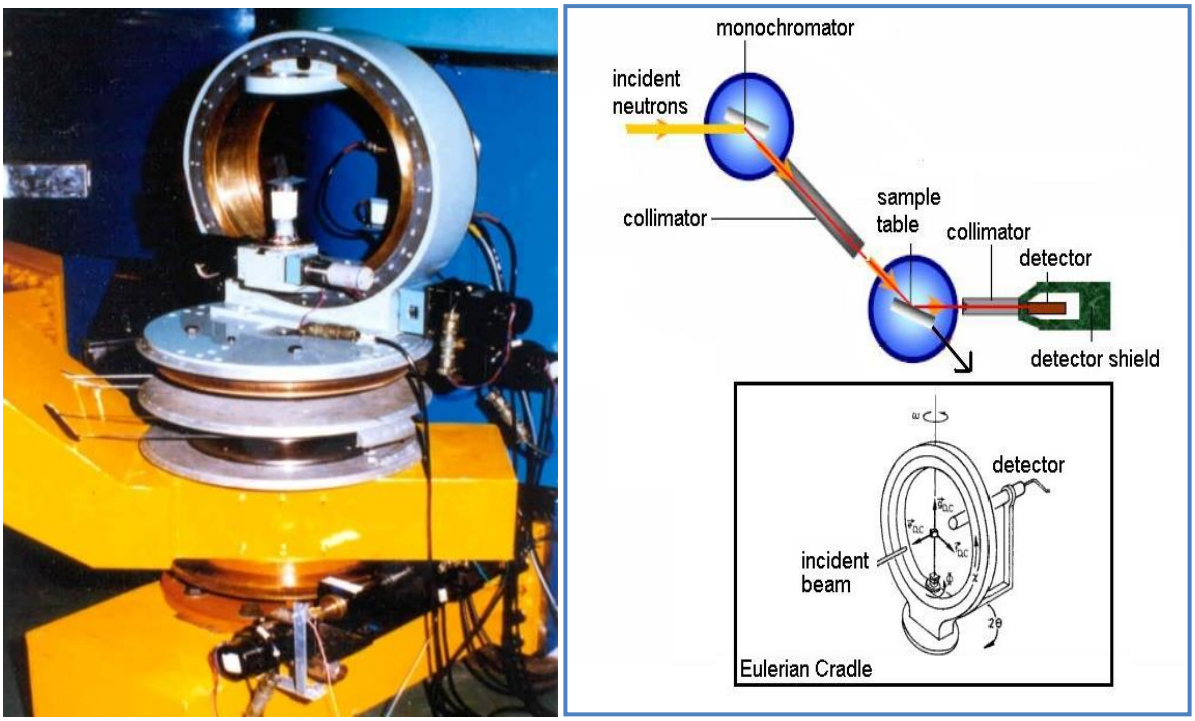

Figure 3. The four-circle diffractometer at Dhruva

The four-circle diffractometer at Dhruva (Figure-3) has an Eulerian cradle as described above, it is mounted in front of the tangential beam hole T1011 of Dhruva Reactor which is a 100MW vertical

Tank type thermal reactor with natural Uranium as fuel Heavy water as moderator as well as coolant [6]. The Instrument details are as following

Table-1

Incident beam	Thermal neutrons of wavelength 0.995Å
Geometry	Four circle Eulerian geometry
Monochromater	Cu220
Neutron Flux at sample position	$5X10^5$ n/cm^2.sec
Detector	BF_3 point detector

3.1 Incident beam: Neutron versus X-rays a comparison

Till now we have discussed the details of single crystal diffraction technique which are equally applicable for both X-ray well as neutron diffraction. Main difference between X-ray diffraction and neutron diffraction results from the difference in the nature of interaction between these incident beams and the scattering atoms [7].

Interaction between X-ray photons and atoms is electrostatic in nature, X-ray photons are mainly scattered by the electrons of the atom, hence what we get at the end of single crystal X-ray diffraction experiment is the electron density within the unit cell. Strength of interaction between X-ray photons and atoms depend directly on the number of electrons present within an atom hence heavier atoms scatter X-ray photons much more effectively than the lighter ones, as a result, positions of lighter elements like Hydrogen, lithium etc are determined to much lesser accuracy as compared to heavier atoms, this is a major disadvantage of single crystal X-ray diffraction experiments. Another disadvantage of single crystal X-ray experiment is that one cannot differentiate between the isotopes of an element using this technique because the different isotopes of an element have same number of electrons. Major advantage of single crystal X-ray experiments is that they require very small single crystals (few micron size crystals) and they can be completed within less than a day, this is mainly because the available X-ray sources are very strong as compared to the available neutron sources.

Interaction between the incident neutrons and scattering atom is nuclear in nature, incident neutron interacts with the atomic nucleus as result we obtain nuclear density from single crystal neutron diffraction experiments. Since the strength of interaction between free neutron and atomic nuclei throughout the periodic table is more or less of same order of magnitude (figure-4), in case of neutron diffraction we do not have the problem of light atoms or heavy atoms as in the case of X-ray diffraction. Hence in this case, positions of all the elements can be detected to the same accuracy irrespective of the atomic weight i.e. both Uranium as well as hydrogen position within a crystal can be obtained accurately using this technique. This is a major advantage in studying structures of crystals containing hydrogen atoms. Moreover one can distinguish between the different isotopes of the elements using this technique since nuclear interaction between a free neutron and nucleus of different isotopes of an element are very different. Major disadvantage of single crystal neutron diffraction experiments is that one requires a very large crystal (of the order of 1mmX1mmX1mm) to get meaningful data and it can take anywhere between few days to weeks to get the complete data set from such crystals, this is mainly because the available neutron sources are orders of magnitude weaker than the available X-ray sources.

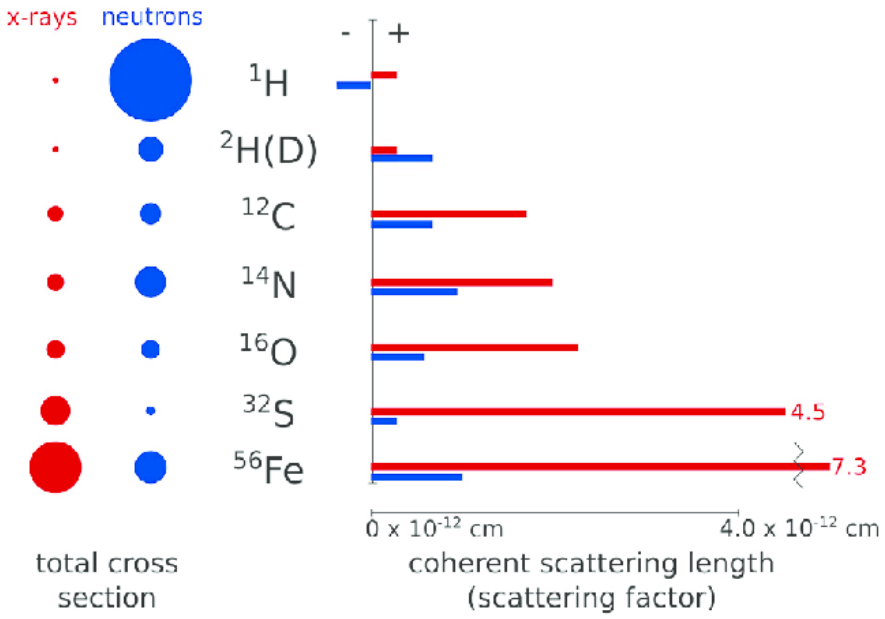

Figure 4. A comparison between the X-ray and Neutron coherent scattering lengths and total scattering cross-sections of commonly occurring elements.

It is important to point out that due to the fundamental difference between the nature of interaction between a beam of monochromatic x-ray photon with matter and a beam of monochromatic neutrons with matter, the coherent scattering length for X-rays is always positive whereas coherent scattering length for neutrons can be positive as well as negative [8] (figure-4). Hence we can have negative scatterer density in Fourier maps obtained using neutron diffraction data but we cannot have such negative scatterer density in X-ray Fourier maps. One of the most important negative scatterer of neutron is the Hydrogen nucleus.

3.2 Hydrogen bond interaction

The unique advantage of single crystal neutron diffraction technique to reliably locate light atoms like hydrogen in the presence of other heavier atoms makes it an important technique in studying hydrogen bonded Materials. This fact can be clearly demonstrated by the help of an example: Crystal structure of bis(glycinium) oxalate was solved both using single crystal X-ray as well as single crystal neutron diffraction methods, Figure-5 shows a difference Fourier map calculated taking all the non-hydrogen atoms of the asymmetric unit, of the plane containing the strong O-H—O hydrogen bond between glycinium and oxalate ions of the crystal. One can see that the electron density around H position obtained from x-rays diffraction is diffuse and extended hence it is difficult to obtain the precise H atom position; in contrast the position of hydrogen atom nucleus can be very clearly located from the neutron diffraction data.

Hydrogen bond is non-covalent intermolecular interactions between an electron deficient hydrogen nucleus and a region of high electron density, It is defined as an attractive interaction (X-H---Y) between a hydrogen atom from a molecular fragment X–H in which X is more electronegative than H, and an atom (Y) or a group of atoms in the same or a different molecule, in which there is evidence of bond formation [9]. The most important criterion used to establish the existence of a hydrogen bond is that the length of the X–H bond increases on hydrogen bond formation and the angle <X-H-Y is close to 180º. This shows that the knowledge of precise H atom position is very important for establishing the existence of hydrogen bonds in materials and single crystal neutron diffraction is the

only technique which gives this information to the require accuracy. As a result, single crystal neutron diffraction is one of the most important technique used in the studies of hydrogen bonded materials like the organic drug molecules, monomeric units of biomolecules like the amino acid and nucleotides, solid state proton conductors used in fuel cells, organic non-linear optic materials etc.

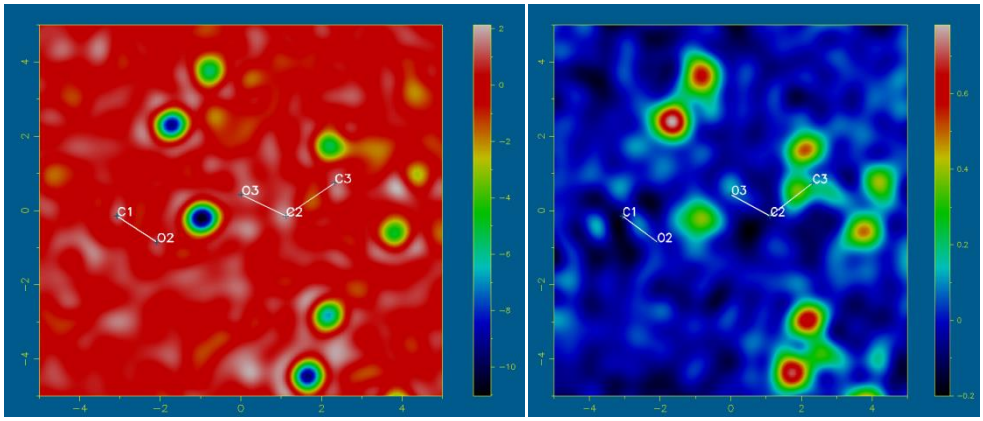

(A) (B)

Figure 5. Difference Fourier map of the plane containing the strong O-H—O hydrogen bond of Bis-Glycinium oxalate of crystal (A) obtained using neutron diffraction data (B) obtained using diffraction X-ray data

4 Neutron crystallographic studies at Trombay: Examples

Neutron crystallography in Bhabha Atomic Research centre started its journey in early sixties. The interest in hydrogen bonded systems led to the development of single crystal neutron diffractometer at Cirus reactor [10, 11]. With the advent of high flux reactor Dhruva in 1985, new fully automated single crystal neutron diffractometer was commissioned at Dhruva which is still operating; its original Pyrolitic graphite monochoromator was replaced by a Cu 220 crystal in 2005 giving a monochromatic neutron beam wavelength of 0.995Å and sin θ/λ range is up to 0.71 $Å^{-1}$. Currently this four-circle neutron diffractometer located at 100 MW Dhruva reactor has a monochromatic neutron flux of 6 x $10^5 n/cm^2/s$, and is routinely used for recording neutron diffraction data, yielding data rates of 25 reflections a day from crystals of small molecules having unit cell sizes less than $1000A^3$. In the following sections we briefly discuss the studies conducted at the 4-circle single crystal diffractometer right from the time of its installation at Cirus up to the current times at Dhruva.

4.1 Hydrogen bonding studies on Crystal hydrates

Water molecule has very interesting hydrogen bonding interaction both as a donor and acceptor of hydrogen bond. Initial studies were on hydrate crystals to study the coordination modes of water molecule using single crystal neutron diffraction [12]. Single crystal neutron diffraction on the following crystals were undertaken. : $K_2C_2O_4$. H_2O, [13]. $Cu(NH_4)$ $SO_4 2H_2O$ [14], $BeSO_4$ $4H_2O$ [15] $K_2Mn(SO_4)_2$ $4H_2O$ [16] , $Ba(ClO_3)_2$ H_2O [17], K_2CuC1_4 $2H_2O$ [18]

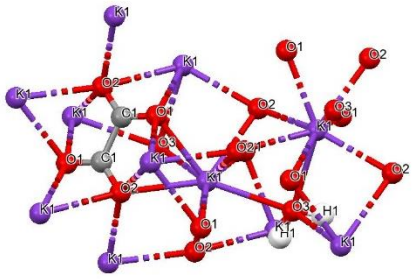

Figure 6. Asymmetric unit of $K_2C_2O_4$. H_2O

These studies provided data regarding the geometry and the flexibility of the O-H---O hydrogen bonds. This was further used to develop improved potential functions for describing the O-H---O hydrogen bonds [19]. The Lippincott Schroeders empirical potential was modified to account for bend hydrogen bonds and potential which included the bend hydrogen bonds was proposed [20]. These studies also led a methodology for classification of the lone pair coordination of water molecules.

4.2 Hydrogen bonding in biomolecules

To obtain accurate position of hydrogen atom and to further analyse stereochemistry and the systematics of hydrogen bonding interaction in amino acid and small peptides, single crystal neutron diffraction was taken up for following crystals *L-Lysine monohydrochloride dehydrate [21]*, *L-threonine* [22], *l-asparagine Monohydrate [23]*, L-Cysteic acid monohydrate *[24]*, *Racemic* dl-Aspartic acid [25], *L-Cystine dihydrochloride* [26*]*, *L-Glutamic acid hydrochloride: [27]*

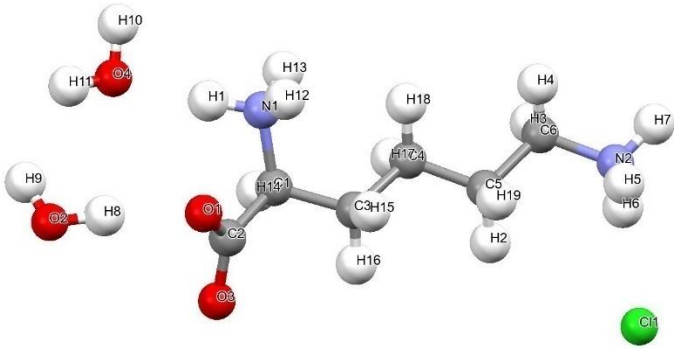

Figure 7. Asymmetric unit of L-Lysine monohydrochloride dihydrate

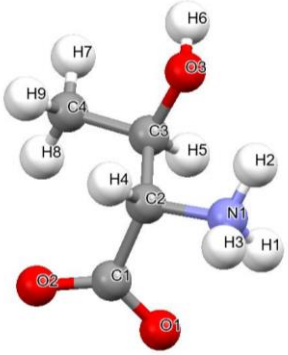

Figure 8. Asymmetric unit.of L-threonine

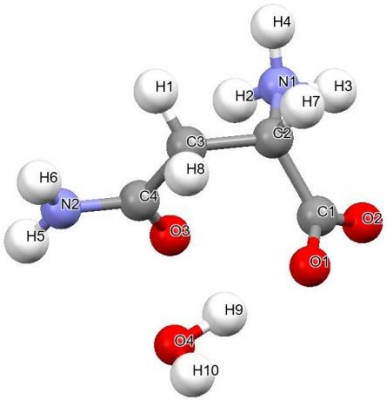

Figure 9. Asymmetric unit of l-asparagine Monohydrate

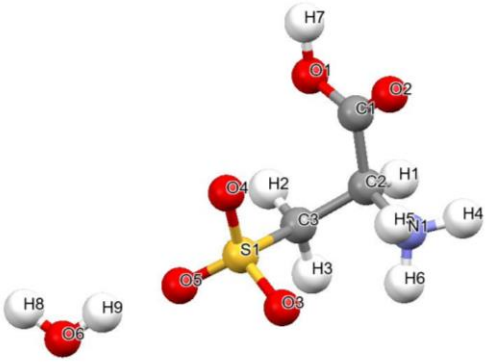

Figure 10. Asymmetric unit of L-Cysteic acid monohydrate

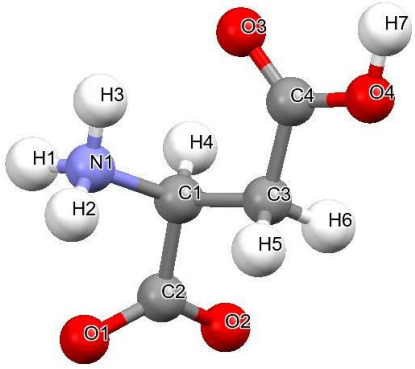

Figure 11. Asymmetric unit of DL-Aspartic acid

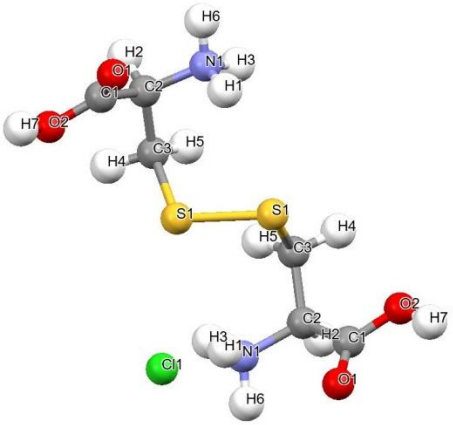

Figure 12. Asymmetric unit of L-Cystine dihydrochloride

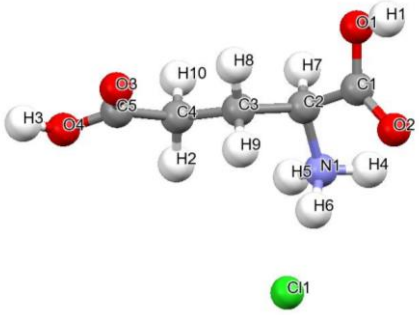

Figure 13. Asymmetric unit of L-Glutamic acid hydrochloride

These molecules have various donor and acceptor groups of hydrogen bonds (X-H…Y). Average values, standard deviations and ranges of values for X-H, H---Y and X... Y distances and the angle at X were obtained for the hydrogen bonds. The inverse correlations between X-H and H---Y, as well as X-H and X... Y were analysed for N-H---O, N-H---O and O-H---O hydrogen bonds. Parameters of the potential functions for O-H---O [19], and N-H---O bonds were updated using the amino-acid data. The information obtained from these crystal structures were used as a database for analysing and optimizing X-ray protein structures.

Mononucleotide 5′-UMP disodium salt

Single crystal neutron diffraction on the mononucleotide5′-UMP disodium salt was carried out. This is the first compound of its class to be probed by neutrons to obtain accurate information on the entire structure. The neutron structure 5′-UMP [fig. 14a) gives better coordinates for hydrogen positions and better hydrogen-bonding parameters. The structure could also distinguish between the sodium ions and the water molecules. Na ions were connected to the main molecule through water molecules and sugar oxygens[fig. 14b). The database study shows that wherever the gauche–gauche conformation of the sugar is encountered, there exists an intramolecular C6–H6...O5′ hydrogen bond [28].

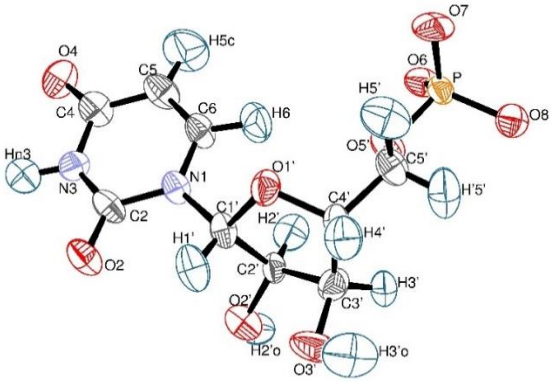

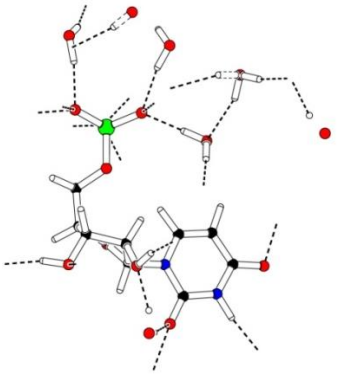

Figure 14a. Asymmetric unit of 5'UMP Figure 14b Water coordination with Sodium

4.3 Hydrogen bonding studies in organic and metalloorganic compounds:

Tetrachlorohydroquinone

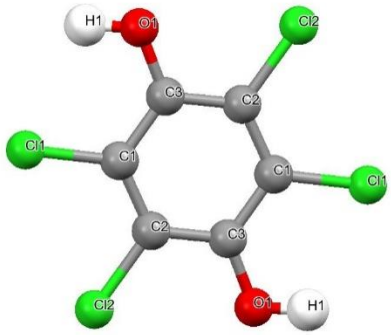

Figure 15. Asymmetric unit of Tetrachlorohydroquinone

The crystal structure of Tetrachlorohydroquinone was studied using single crystal neutron diffraction. The heavy atom positions agreed with that of X-ray structure, the hydrogen atom positions were displaced by 1 Å. The proposed bifurcated hydrogen bond interaction using X-ray structure did not exist, rather there was a closed packed layer of molecules parallel to (100) plane with six-fold coordination of each molecule. The layers were connected by O-H…O hydrogen bond [29].

Bis (Hydrogen maleato)-tetra-aqua-zinc(ii) and Bis(Hydrogen maleato)-tetra-aqua-nickel(ii)

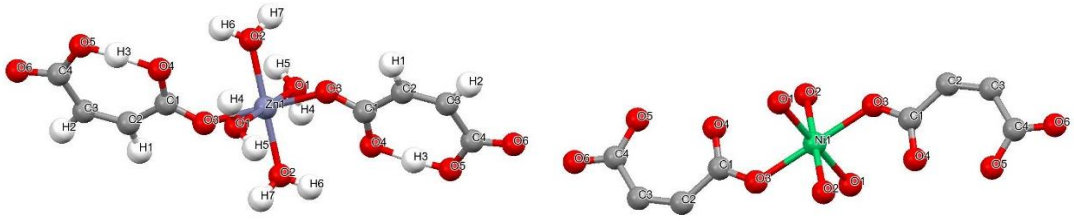

Figure 16. (a) Asymmetric unit of bis(Hydrogen maleato)-tetra-aqua-zinc(ii) (b) bis(Hydrogen maleato)-tetra-aqua-nickel(ii)

The structure of the hydrogen maleate ion has been the subject of great interest in order to investigate the influence of counter ions and packing on the geometry and internal hydrogen bond. The single crystal neutron diffraction of 2 bis(Hydrogen maleato)-tetra-aqua-zinc(ii) and bis(Hydrogen maleato)-tetra-aqua-nickel(ii) was taken up. It was found that the neutron model of the Zn salt and the high-order model of the Ni salt show great similarity. The hydrogen maleato geometry proved to be independent of the nature of the counter ion; Differences between Zn—O and the corresponding Ni--O distances are (much) larger, partly reflecting the difference in effective ionic radii of Zn^{ii} and Ni^{ii}. Hydrogen bonding reduces the symmetry of the metal coordination from O_h to C_i, and that of the hydrogen maleate ion from C_{2v} to C_1. A three-centre bifurcated donor hydrogen bond is observed. A very short [2.410 (4)A] asymmetric intramolecular hydrogen bond is found (O--H = 1.097Å, O...H = 1.316 Å) [30]

Semicarbazide hydrochloride and Hexa deuteron semicarbazidium chloride

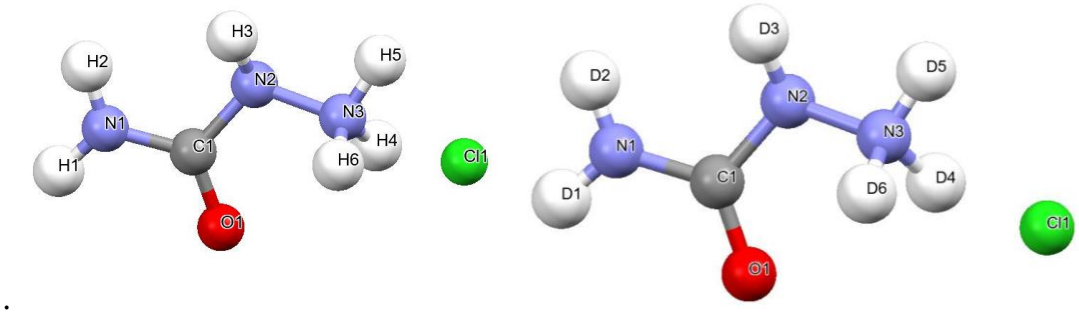

Figure 17. (a) Asymmetric unit of Semicarbazide hydrochloride, and (b) Asymmetric unit of Hexa deuteron semicarbazidium chloride

Semicarbazide is used in preparing pharmaceuticals including nitrofuran antibacterials (furazolidone, nitrofurazone, nitrofurantoin) and related compounds. The structure is held together by a three-dimensional network of N-H...CI and N-H...O hydrogen bonds. Two hydrogens of $-NH_3^+$ and one of the $-NH_2$ groups are strongly hydrogen-bonded to the chloride ions, while the third hydrogen of the $–NH_3$ and the amino hydrogen are bonded to the neighbouring carboxyl oxygens. The non-centrosymmetric space group $P2_12_12_1$ determined in the present studies at 298 (1)K suggested no ferroelectric-paraelectric (FE-PE) transition in this compound. It was also observed from the structure of Hexa deuteron semicarbazidium chloride that the effect of deuteration on hydrogen-bond dimensions is more than the effect on valence-bond dimensions, consistent with atomic orbital theory. Existing data support the fact that the replacement of H by D does result in elongation of hydrogen-bond lengths. It was concluded that there is no ferroelectric phase transition in these materials between 123 and 323 K [31, 32]

4.4 Phase transition in $LikSO_4$

Lithium potassium sulphate ($LiKSO_4$) crystals present a rich sequence of phase transitions over a large temperature range from 30K up to almost 943K. Systematic studies on the low temperature phase transitions in LiKSO4, were obtained from single crystal neutron diffraction measurements. The study indicated three clear phase transitions at 205 K (from sp. gr. P6, to sp. gr. P31c), at 189 K (to sp. gr. Cc) and 135 K in the cooling cycle; a phase change is also indicated at 165K. All these transitions show thermal hysteresis. The full crystal does not undergo transformation at any of the

transition temperatures but exhibits mixed phases. The kinetics of the phase transitions are characterised by prolonged equilibration times (days) which strongly depend on the thermal history of the sample. With the results of the structural investigations in the temperature range 300K to 100K, an attempt was made to explain the anomalies and variant results observed in the physical properties of $LiKSO_4$, at low temperatures [33, 34, 35]

4.5 Phase transition studies in Ferroelectric, optoelectronic and piezoelectric crystals

Structural phase transition and single-crystal neutron diffraction study of ferroelectric $Ba_{0.92}Ca_{0.05}TiO_3$

Crystal structure of $BaTiO_3$ doped with 8% Ca^{2+} is refined using single-crystal neutron diffraction data and it is shown that the doped Ca^{2+}ion substitutes only at the Ba sites. The refined cell (P4mm) parameters are a = b = 3.982(3)Å c= 4.003(3) Å with a final R value of 0.02 (on F). Existence of multiple domains in the crystal was ruled out based on refinement with multidomain model [36] The tetragonal-to-cubic transition in ferroelectric $Ba_{0.95}Ca_{0.05}TiO_3$ (BCT) has been studied using a single-crystal neutron diffraction technique. The intensities of the Bragg profiles are observed to increase anomalously with temperature above 110°C and then to drop sharply before reaching the structural transition temperature T0. The intensity variations and T_0 are sensitive to sample heating rate with T_0= 145°C at slow heating rates. Structural refinements indicate that the observed intensity variations are due to changes in the domain structure and the thermal parameters B with the latter becoming anomalously large several degrees Celsius below T_0 compared with those above T_0 and at room temperature, indicating the onset of significant pretransition disorder for Ti ions along the polar c axis. The observed linewidths of the diffraction profiles reflect contributions from the anisotropic domain sizes and the internal strains and an added contribution from the coexistence of tetragonal and cubic phases below T_0. The results suggest that the fluctuations in the Ti positions existing well below T0 could be responsible for the broadening of dielectric response observed for BCT [37]

Zinc (tris) thiourea sulphate (ZTS)

Zinc(tris) thiourea sulphate, $Zn(SC(NH_2)_2)_3SO_4$ (ZTS) is metal-organic crystal which is used for electro-optical (EO) applications and frequency doubling of near IR laser radiations. In this study, the crystal structure of ZTS[fig. 18] has been obtained in detail by single crystal neutron diffraction technique. ZTS crystallizes in non-centrosymmetric symmetry with four formula units in the unit cell. The structure comprises three thiourea (tu) groups (tu1, tu2, tu3) and
$(SO_4)^{2-}$ ions. Using the structural parameters and an existing formalism based on the theory of bond polarizability, the contributions from each of the structural groups in the unit cell to the total values of the EO coefficients of ZTS were estimated. The total linear susceptibility (χ) and the ionic components (rijk) ion for the crystal are estimated by summation of the respective values for each bond. The electronic components $(rijk)^{el}$ are calculated from the measured NLO coefficients. These results showed that the tu1, tu2, tu3 and $(SO_4)^{2-}$ groups contribute about 17% to the total value of χ whereas a maximum of about 25% contribution arises from the H-bonds alone. Thus the present work points out the molecular groups are relatively more sensitive to the EO coefficients. This helps to grow crystals with better linear optical and EO properties. It also demonstrates the importance of neutron diffraction technique, which gave better information on the H-atoms [38]

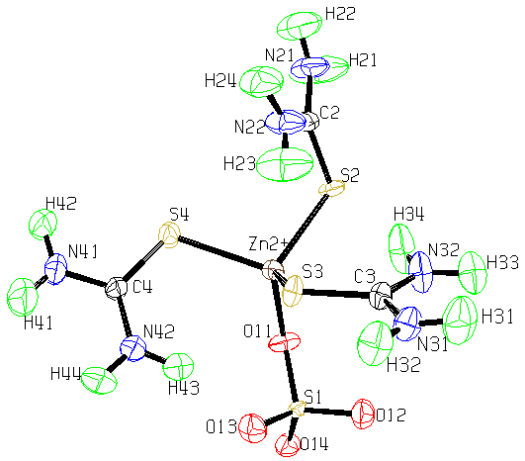

Figure 18. Asymmetric unit of Zinc (tris) thiourea sulphate (ZTS)

Triglycine sulphate

Triglycine sulphate ($(NH_2CH_2COOH)_3H_2SO_4$) is one of the important and well studied ferroelectric crystals of great technological relevance. In triglycine sulphate (TGS), crystal structure and physical properties are primarily affected by the hydrogen bond interactions between three glycine ions, namely GI, GII and GIII and the tetrahedral negative acidic residue ions SO_4. Hence it is important to know the exact hydrogen-bonding scheme in these crystals in order to understand and modify their properties. With an intention to get the exact hydrogen atom positions in TGS crystals, neutron diffraction study on TGS was taken up. Since no field was applied during the data collection, the crystal was not single domain but instead both the domains were found to be present with occupancy 88% and 12%. The most important difference is found in the short hydrogen bond (O10–H7–O8) connecting GIII and GII, the O10- - -O8 distance is found to be 0.031 Å smaller than that reported by the earlier neutron study [fig. 19]. The O10–H7–O8 bond connecting GII and GIII has an energy contour having a single minimum and asymmetric [39].

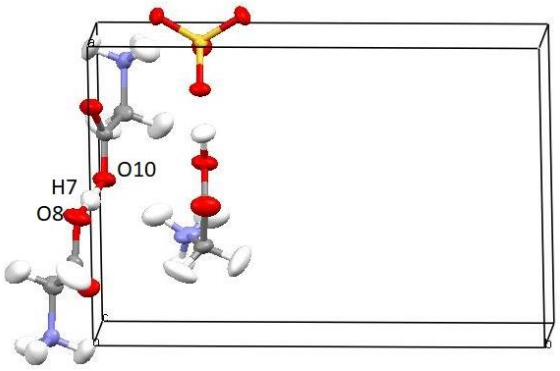

Figure 19. Asymmetric unit of Triglycine sulphate

Triglycine selenate

The phase transition in TGSe which is known to be structurally isomorphous to TGS is not as clearly understood as that of TGS. The tricritical nature of the ferroelectric phase transition in TGSe has led to a resurgent interest in phase transition studies on this class of hydrogen bonded ferroelectric crystals. Single crystal neutron diffraction of TGSe was undertaken at RT which is the paraelectric phase. The most important conclusion derived from the comparison between the unit cell parameters of TGSe and TGS is that substitution of a SO_2^{-4} ion (molecular volume 62.0 $Å^3$) by a larger SeO_2^{-4}

ion (molecular volume 66.8 $Å^3$) results in a swelling of the unit cell, as is evident by the increase in the lengths of the unit cell vectors a, b and c, although there is no change in the shape of the unit cell since angles α, β, γ remain unchanged. This substitution can be equated to a net effective chemical pressure, which dilates the unit cell. The nitrogen atom N1 of GI is disordered about the b-plane, the elongated shape of its thermal ellipsoid suggests that the disorder is in all likelihood dynamic[fig. 20]. The hydrogen atom between GII and GIII occupies a symmetric position between the two molecules; its thermal ellipsoid is also elongated along the line joining the two molecules, indicating dynamic disorder [40]

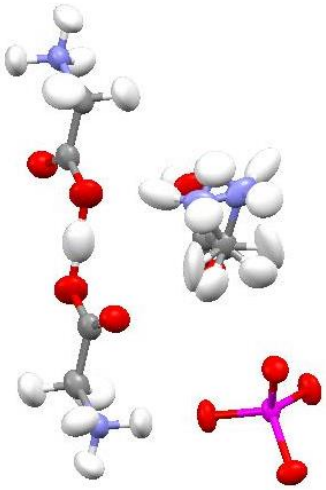

Figure 20. Asymmetric unit of Triglycine selenate

TGS doped with alanine (LATGS)

One of the major limitations of detectors made of TGS crystals is depoling of TGS with time , Alanine substitution is one of the ways to prevent depoling in TGS It is believed that the Alanine molecule, which is very similar to the Glycine molecule, enters the unit cell of TGS as a substitution to one of the three glycine molecules, namely glycine-1, glycine-2 and glycine-3, and prevents the reversal of polarization in the cell. The effect of Alanine substitution is known to be similar to the application of an external field to a pure TGS crystal .In order to understand how Alanine substitution prevents depoling in TGS ,single crystal neutron-diffraction study was undertaken to find the site of the alanine substitution. The very small difference between the cell parameters of TGS (a = 9.417 Å, b = 12.643 Å, c = 5.735 Å, β = 110.4 deg) and those of LATGS (a = 9.444(5) Å, b = 12.661(19) Å, c = 5.751(3) Å, β = 110.34(2) deg), supported the assumption that alanine enters as a substitution in some of the unit cells of the crystals. Results of our refinement indicated that substitution might be at the zwitterionic site G2 of our structure, although concrete evidence in the form of significant peaks in the difference Fourier map was not obtained. An Alanine molecule at the site G2 has short steric contacts with the $–NH_3$ group of glycine-1 in one of its equivalent positions; as a result in the unit cells in which Alanine is present instead of glycine at the G2 site glycine-1 is forced to occupy the G1 position only it cannot occupy the G1’ position [fig. 21]. Hence one of the polarization directions is frozen in such unit cells [41]

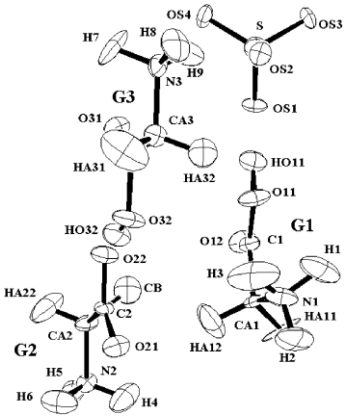

Figure 21. Asymmetric unit of Triglycine sulphate doped with alanine

Langasite family: A comparative study

Crystals of the langasite family are of interest as they are used as piezoelectric in different devices. The properties of these classes of crystals can be modified within certain limits by isomorphous substitution. Single-crystal neutron diffraction studies were carried out for LGT ($La_3Ga_{5.5}Ta_{0.5}O_{14}$), LGST ($La_3Ga_{5.25}Ta_{0.25}Si_{0.5}O_{14}$) and LGZrT ($La_3Ga_{5.25}Ta_{0.25}Zr_{0.5}O_{14}$) as the neutron study gives a better average picture of the crystal properties over a macroscopic region of the grown crystal. The effect of small substitutions at various sites on the piezoelectric properties of the crystal was studied. These crystals have very slight structural differences resulting from the difference in composition. These small structural changes are enough to bring about a noticeable change in their piezoelectric properties. This study attempts to correlate these structural changes to the changes in the material properties. It is shown that the significant change in the Dsite affects the orientation of the A site along the [100] direction leading to a change in the piezoelectric property[fig, 22] [42]

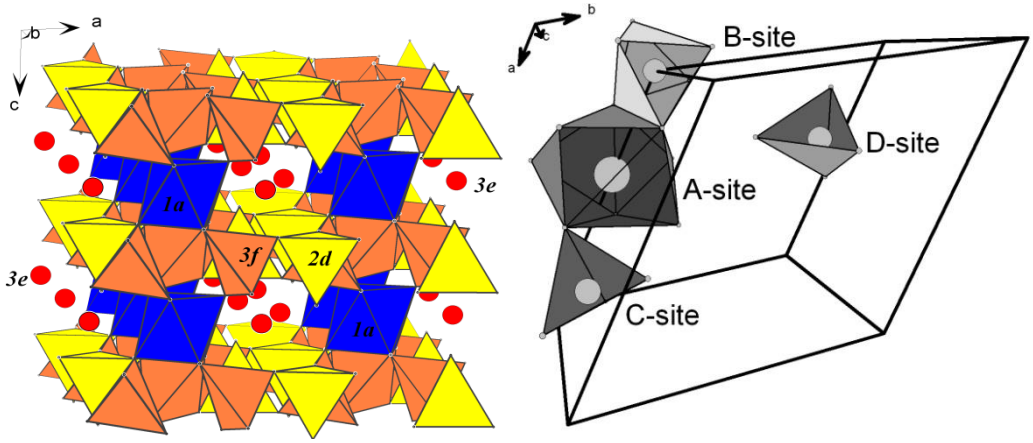

Figure 22. Crystal structure of *Langasite family*

α-Nickel sulfatehexahydrate(NSH) crystals

NSH is a crystal which possesses high transmission efficiency (>80%) in the narrow range 250–340 nm, moderate transmission at 450–600 nm and strong absorption over all other wavelengths. It is therefore considered an ideal candidate for UV light filters. Ultraviolet light filters and UV sensors made of NSH crystals are already commercially available, but low thermal stability and cleavability

are major drawbacks of the NSH crystals. Hydrogen bonding is known to play a crucial part in determining the crystal properties of NSH. Study on -nickel sulfate hexahydrate (NSH)[fig. 23] crystals grown from two different aqueous solutions, one of them containing an excess of sulfuric acid was taken up. Single crystal neutron diffraction showed subtle differences in the SO_4 geometry and the intramolecular separation between the SO_4^{2-} and $[Ni(H_2O)_6]^{2+}$ ions of the NSH molecule. This is found to be due to the solvent effect, where addition of sulfuric acid to the crystallization solution alters the solvent properties of water in such a way that its screening effect and hence its salt solubility decreases. This leads to the fine-tuning of interionic interaction between SO_4^{2-} and $[Ni(H_2O)_6]^{2+}$ ions in the solution phase, and this feature is carried over into the crystalline phase [43].

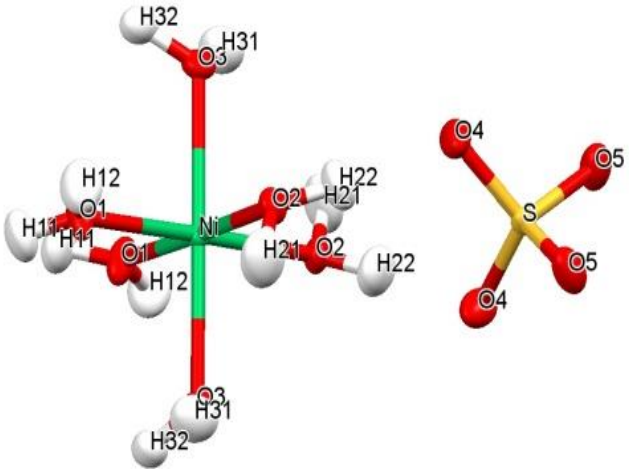

Figure 23. Asymmetric unit of α-Nickel sulfatehexahydrate(NSH) crystals

Ammonium dihydrogen phosphate(ADP) : potassium dihydrogen phosphate KDP mixed crystals

Proton dynamics plays a key role in the structural ferroelectric (FE)/antiferroelectric (AFE) phase transition in the crystals belonging to the potassium dihydrogen phosphate crystal family. Mixed crystals belonging to this family having the composition $M_{1-x}(NW_4)_xW_2AO_4$, where M = K, Rb, Cs, W = H, D, and A = P,As, exhibit proton glass behavior due to frustration between FE and AFE ordering; these proton glasses do not undergo any structural phase change but retain their room temperature structure down to very low temperatures. Single crystal neutron diffraction investigations of four mixed crystals with composition ($K_{1-x}(NH_4)_xH_2PO_4$), where x = 0.0, 0.29, 0.67 1.0,were undertaken with the intention to investigate the effect of the local structural deviations on the overall average structure of the crystals and correlate these structural changes to the presence or absence of a structural phase transition in these crystals. Hydrogen bonding is shown to play a key role in the changing nature of the mixed crystals as the composition varies from the potassium rich ferroelectric region to the proton glass region to the ammonium rich antiferroelectric region [44].

Single crystal neutron structure of (K)0.25(NH 4)0.75 H 2 PO 4 mixed crystals was obtained and compared with previously determined structures of KDP_X ADP $_{1-X}$ crystals. Basic structural framework of crystals belonging to potassium dihydrogen phosphate family is constructed by a network of zigzag O–H–O hydrogen bonded chains of PO_2 (OH) $_2$ anions, with cations occupying the interspaces of the zigzagged anionic chains. These crystals having simple crystal structure primarily determined by the O–H–O hydrogen bonds connecting PO_2 (OH) $_2$ anions provide us with a unique opportunity to tune the hydrogen bond geometry by varying the cationic occupancy and study the

effect of this change on the average structure of the crystal. The cation–anion interaction is found to have a direct influence on the O–H–O hydrogen bonds of the mixed crystals. [45]

Effect of deuteration On ADP and KDP Crystals

Single-crystal neutron diffraction investigations on ADP and KDP crystals along with their deuterated analogue crystals under ambient conditions was carried out. Primary isotope effect on O–H bonds in ADP is approximately four times that in KDP, i.e. the change in O–H bond length on deuteration is significantly higher in ADP than in KDP. This indicates that the O–H covalent bonds in ADP are less stiff and hence weaker than those in KDP. This is a direct consequence of the partial covalent nature of the NH_4 –O interaction in ADP, leading to charge redistribution between the ammonium ion (NH_4) and the O atom, thereby weakening the O–H bonds and making them more polarisable. This reduced the bond stiffness and hence the increased bond polarisability in ADP and is most likely responsible for the NLO coefficient to be larger in ADP than in KDP.• The secondary isotope effect defined as the change in O–O distance of O–H–O hydrogen bond on deuteration is found to be higher in KDP than in ADP. Small secondary isotope effect in ADP compared to that in KDP is an indication of a stronger O–H–O hydrogen bond in ADP. It is proposed that the presence of a partially covalent $N–H_N$ –O bond in ADP has a very significant effect on its O–H bond making it highly anharmonic [46].

Thiourea-doped ammonium dihydrogen phosphate:

Ammonium dihydrogen phosphate (ADP) belongs to the isomorphous series of phosphates and arsenates of which potassium dihydrogen phosphate (KDP) is a member. Both KDP and ADP are well known for their nonlinear optical and piezoelectric properties. The difference between KDP and ADP is undoubtedly attributed to the presence of NH^+_4 ions, which allow for the possibility of forming an extra hydrogen bond between N and O in ADP. A small amount of thiourea in ammonium dihydrogen phosphate (TADP) results in a significant change in the properties of ADP, for example, the second harmonic generation efficiency of TADP crystals is three times that of ADP crystals. Single crystal neutron diffraction investigation on TADP crystals was undertaken to investigate the changes in the hydrogen bonding of the system. Though the dopant (thiourea) could not be located from the difference Fourier map, the cell parameters of TADP were found to be significantly different from that of pure ADP at RT. It is interesting to note that the change is mainly in a and b parameters whereas c remains almost unchanged, and as a result the c/a ratio of ADP reduces on doping. It was observed that there is significant increase in the N and O distances in TADP crystals. This indicates that the average strength of N–H- - -O bonds reduces in TADP as compared to that in ADP[fig. 24]. The observation that paraelectric–antiferroelectric phase transition in TADP does not take place even till 116 K can be rationalized by the fact that the strength of N–H- - -O in TADP is significantly reduced as compared to that in ADP [47].

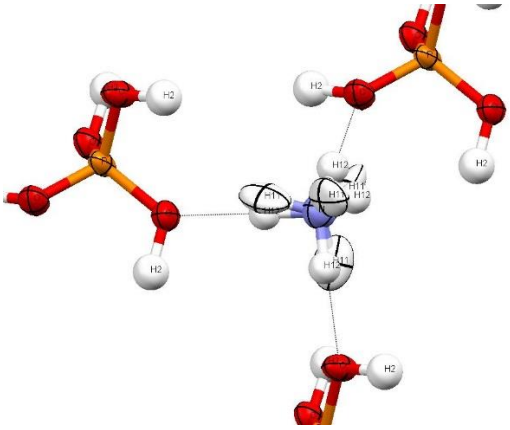

Figure 24. Asymmetric unit of Thiourea-doped ammonium dihydrogen phosphate

4.6 Proton Conductors

Effect of cationic substitution on the double-well hydrogen-bond potential in $[K_{1-x}(NH_4)_x]_3H(SO_4)_2$ proton conductors:

The structure of the mixed crystal $[K_{1-x}(NH_4)_x]_3H(SO_4)_2$ as obtained from single-crystal neutron diffraction[fig. 25] is compared with the previously reported room-temperature neutron structure of crystalline $K_3H(SO_4)_2$. The two structures are very similar, as indicated by the high value of their isostructurality index (94.8%). It was found that the replacement of even a small amount (3%) of K^+ with NH^{4+} has a significant influence on the short strong hydrogen bond connecting the two SO_4^{2-} ions. Earlier optical measurements had revealed that the kinetics of the superionic transition in the solid solution $[K_{1-x}(NH_4)_x]_3H(SO_4)_2$ are much faster than in $K_3H(SO_4)_2$; this reported difference in the kinetics of the superionic phase transition in this class of crystal was explained on the basis of the difference in strength of the hydrogen-bond interactions in the two structures [48].

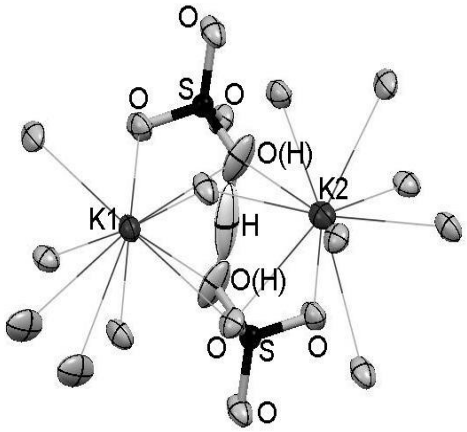

Figure 25. Asymmetric unit of $K_{1-x}(NH_4)_x]_3H(SO_4)_2$ proton conductors

Deterioration of hydrogen-bonded superprotonic conductors belonging to $CsHSO_4$–CsH_2PO_4–H_2O salt system

Single-crystal neutron diffraction investigation on $Cs_4(HSO_4)_3(H_2PO_4)$ and $Cs_6H(HSO_4)_3(H_2PO_4)_4$ superprotonic crystals, belonging to $CsHSO_4$ –CsH_2PO_4 –H_2O salt system, is under taken to elucidate the precise hydrogen atom positions in these crystals. The investigation revealed that these crystals are very sensitive to the ambient conditions and can undergo deterioration due to fluctuation in air moisture content. $Cs_6H(HSO_4)_3(H_2PO_4)_4$ crystals are more stable as compared to $Cs_4(HSO_4)_3(H_2PO_4)$. Crystal

structure of $Cs_6H(HSO_4)_3(H_2PO_4)_4$ [fig. 26]is obtained both before and after deterioration, it is found that the asymmetric O–H…O hydrogen bond between the PO_4 and SO_4 ions of this crystal becomes stronger after deterioration. This led to the shrinkage of the unit cell, and most likely prevented further deterioration. Diabatic state model for hydrogen bonds is used to obtain the energy contour for the O–H…O hydrogen bond of $Cs_6H(HSO_4)_3(H_2PO_4)_4$ crystal [49]

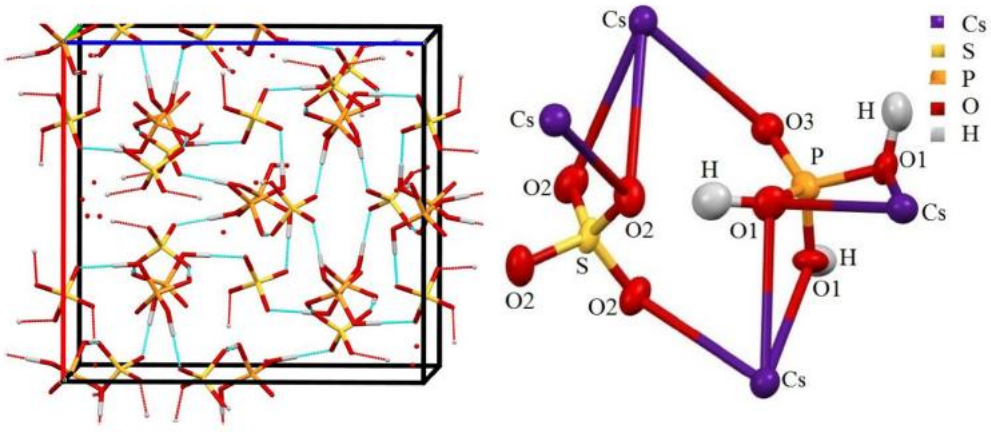

Figure 26. Asymmetric unit of $CsHSO_4$–CsH_2 PO_4–H_2O salt system

4.7 Hydrogen Bonding studies on Amino acid- Acid cocrystals.

Bis(glycinum) oxalate

Single-crystal neutron diffraction investigation of bis(glycinium) oxalate was undertaken in order to study its hydrogen bonding network, particularly the very short hydrogen bond between the glycinum and oxalate ions, indicated by the X-ray diffraction study. The non-existence of any phase transition in these crystals was attributed to the fact that the short hydrogen bond in bis(glycinium) oxalate is asymmetric in nature, with no hydrogen disorder[fig. 27]. The potential energy landscape for the above-mentioned H atom was found to have a single minimum closer to the glycinium ion. [50].

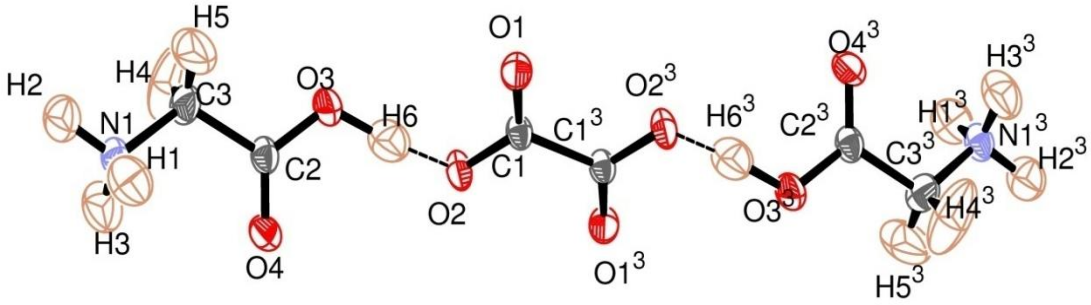

Figure 27. Asymmetric unit of Bis(glycinum) oxalate

L-Histidine nitrate

Crystal structure of L-histidine nitrate was obtained using single crystal X-ray and neutron diffraction, the asymmetric unit consists of imidazole ring of L-histidine in biprotonated state, the amino group also in protonated state with the carboxylic group in deprotonated state, L-histidine molecule adopts gauche (-) conformation. Cambridge Structural Database was used to search complexes of Histidine with nitrates, a comparison of the of structural parameters and intermolecular interactions of four

complex DL Histidinium dinitrate, L-histidinium nitrate monohydrate, L-histidinium dinitrate and our complex L-Histidine nitrate showed that only in L-histidine nitrate monohydrate the Histidine molecule adopts Gauche(+) conformation. A comparison of globularity parameter amongst the four above mentioned structures revealed that L-histidine nitrate monohydrate shows maximum globuarity and asphericity of our structure (L-histidine nitrate) is prolate in nature. Also the intermolecular interaction studied through Hirshfeld analysis showed that L-hisitidine nitrate monohydrate has maximum percentage of H..H interactions. A comparison of the contacts using the x-ray and neutron structure of our complex L-Histidine nitrate showed that maximum change is reflected in the C…H and H…H contacts with C…H having a higher percentage and H…H having a lower percentage in the neutron structure, indicating that the neutron diffraction maps shows the hydrogen bond interaction more accurately . L_hsitidine nitrate monohydrate has higher Energy Gap, ΔEg and also higher average β and hence it is one of the most stable and better material suitable amongst the three for NLO properties [51].

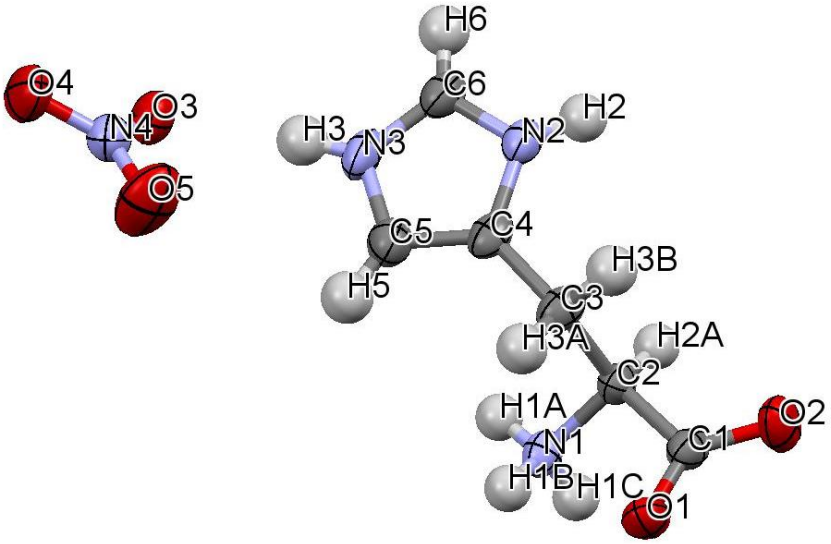

Figure 28. Asymmetric unit of L-Histidine nitrate

5 Summary

Single crystal neutron diffraction is a powerful technique used to unravel the structural details of hydrogen bonded crystals. The four-circle diffractometer at Dhruva has been extensively used over last several years to study the crystal structure of various classes of hydrogen bonded crystals. As shown in this Review, this has led to enormous improvement in our understanding of hydrogen bonded interaction in crystals.

6 References

1) Introduction to solid state physics, C. Kittel, (8th ed.), (2004). John Wiley & Sons.
2) Xray Structure Determination ; A practical Guide, G. H. Stout and L. H. Jensen (2nd ed.) (1989)John Wiley & Sons
3) Phase Problem in X-ray Crystallography, and Its Solution, K. Cowtan, (2001) Encyclopedia of Life Sciences, 1
4) Direct methods in crystallography, M. M. WOOLFSON, (1971) Rep. Prog. Phys., 34, 369-434
5) Crystal structure refinement with SHELXL, G. M. Sheldrick Acta Cryst (2015) C71 3-8

6) Research reactors in BARC: history, development and utilization, K. Chakrabarty & C.G. Karhadkar, (2021). BARC Newsletter, (376), 27-31.
7) Present Needs and Future Trends in Neutron Crystallography and Spectroscopy, (1978) A Workshop sponsored by the Argonne National Laboratory National Science Foundation November 15—17,
8) Investigating Structure and Dynamics of Proteins in Amorphous Phases Using Neutron Scattering, M. M. Castellanos , A. McAuley , J. E. Curtis (2016) Computational and Structural Biotechnology Journal ,
9) Definition of the hydrogen bond (IUPAC Recommendations 2011) (2011) E. Arunan , G. R. Desiraju , R. A. Klein , J. Sadlej , S. Scheiner , I. Alkorta , D. C. Clary , R. H. Crabtree , J. J. Dannenberg , P. Hobza , H. G. Kjaergaard , A. C. Legon , B. Mennucci ,and D. J. Nesbitt Pure Appl. Chem., 83, pp. 1637–1641
10) Trombay automatic diffractometers: a 3-dimensional fully automatic neutron diffractometer. A. Sequeira, S.N. Momin and R. Chidambaram, Indian Journal of Pure and Applied Physics 12 (1974) 121 – 128.
11) An on-line TDC-312 computer controlled neutron diffractometer, A. Sequeira, S.N. Momin. H. Rajagopal. J.N. Soni, R.Chidambaram. Dilip Kumar, A Ramana Rao and V.M. Gopu, Pramana,10 (1978) 289-302.
12) Neutron-Diffraction Study of the Structure of Potassium Oxalate Monohydrate: Lone Pair Coordination of the Hydrogen-Bonded Water Molecule in Crystals, R. Chidambaram, A. Sequeira, and S. K. Sikka, J. Chem. Phys. 4 (1964), 3616–3622.
13) Neutron Diffraction Refinement of the Structure of Potassium Oxalate Monohydrate, A.Sequeira, S. Srikanta and R. Chidambaram, Acta Cryst. B26 (1970) 77
14) Disorder of ammonium ions in di-ammonium tetra-chlorocuprate dihydrate, $(NH_4)_2CuCl_4.2H_2O$: a high-precision neutron diffraction study S. N. Bhakay-Tamhane, A. Sequeira and R. Chidambaram Acta Cryst B36 (1980) 2925-2929
15) A Neutron Diffraction Determination of the structure of Beryllium Sulphate Tetrahydrate Be SO_4. $4H_2O$, S.K Sikka and R. Chidmabaram, Acta Cryst B25 (1969) 310-315
16) Neutron diffraction study of the space group and structure of manganeseleonite, $K_2Mn(SO_4)_2.4H_2O$, S. Srikanta, A. Sequeira and R. Chidambaram, Acta Cryst B24 (1968) 1172-1175
17) Neutron-Diffraction Refinement of the Crystal Structure of Barium Chlorate Monohydrate $Ba(ClO_3)_2 \cdot H_2O$, S.K Sikka, S.N. Momin, H. Rajagopal, and R.Chidambaram, J. Chem. Phys. 48 (1968) 1883–1889
18) Neutron diffraction refinement of the crystal structure of potassium copper chloride dihydrate, K2CuCl4.2H2O, R. Chidambaram, Q.O. Navarro, A. Garcia, K Linggoatmodjo, L. Shi-Chien, L, I.-H. Suh A. Sequeira, S. Srikanta, S. Acta Cryst. B 26 (1970) 827-830
19) Bent O-H…O Hydrogen Bonds in Crystals, R. Chidambaram and S.K. Sikka, Chemical Physics Letter 2 (1968) 162-165
20) Potential functions for hydrogen bond interactions I. A modified lippincott-schroeder potential function for NH···O interaction between peptide groups, R.Chidambaram, R.Balasubramanian, G.N. Ramachandran, Biochimica et Biophysics Acta 221 (1970) 182-195
21) A Neutron Diffraction Study of the Structure of L-Lysine Monohydrochloride Dihydrate R. R. Bugayong, A.Sequeira and R. Chidambaram, *Acta Cryst.* B28 (1972) 3214-3219
22) Structure determination of L-threonine by neutron diffraction, M. Ramanadham, S.K. Sikka and R. Chidambaram Pramana 1 (1973) 247-259
23) Structure of l-asparagine monohydrate by neutron diffraction, M. Ramanadham, S.K. Sikka and R. Chidambaram. ActaCryst. B28 (1972) 3000–3005
24) Refinement of hydrogen-atom positions in L-cysteic acid.H20 from neutron diffraction data. Ramanadham, M., Sikka, S. K. & Chidambaram, R. Acta Cryst. B29 (1973) 1167–1170

25) A Neutron Study on the Structure of DL-Aspartic Acid, A. Sequeira, H.Rajagopal, M. Ramanadham Acta Cryst. C45 (1989) 906-908
26) A Neutron Diffraction Study of the Structure of L-Cystine.2HCl Gupta, S. C., Sequeira, A. & Chidambaram, R. Acta Cryst. B30 (1974) 562-567.
27) A Neutron Diffraction Study of the Structure of L-Glutamic_Acid .HCl, A. Sequeira, H. Rajagopal and R. Chidambaram, Acta Cryst. B28 (1972) 2514
28) Hydrogen bonding in the neutron structure of the mononucleotide 5′-UMP disodium salt, R. Chitra, R. Ranjan-Choudhury, M. Ramanadham, Appl. Phys. A 74 [Suppl.] (2002) S1576–S1578
29) Neutron diffraction study of the hydrogen bond system in tetrachlorohydroquinone S.K.Sikka, R.Chidambaram Acta Cryst., 23 (1967) 107
30) Tetraaquabis(hydrogen maleato)zinc(II) by Neutron Diffraction and Tetraaquabis(hydrogen maleato)nickel(II) by High-Order X-ray Diffraction A. Sequeira, H. Rajagopal, M. P. Gupta, F. Vanhouteghem, A. T. H. Lenstra and H. J. Geise, *Acta Cryst. C48* (1992) 1192-1197
31) A Neutron Structural Study of Semicarbazide Hydrochloride, B. K. Roul, R. N. P. Choudhary H. Rajagopal and A. Sequeira, Acta Cryst. C43 (1987) 668-670
32) A Neutron Diffraction Study of Deuterated Semiearbazide Hydroelfloride, B. K. Roul, R. N. P. Choudhary H. Rajagopal and A. Sequeira Acta Cryst. C44 (1988) 1244-1246
33) Kinetics and symmetry changes in low temperature phase transitions in LiKSO4, Sandhya Bhakay-Tamhane & A. Sequeira, Ferroelectrics 69 (1986) 241-251
34) Low-temperature phase transitions in $LiKSO_4$: A neutron study, Sandhya Bhakay-Tamhane, A. Sequeira and R. Chidambaram, Solid State Communications, 53 (1985) 197-200
35) Structure of Lithium Potassium Sulphate, LiKSO4: A Neutron Diffraction Study S. Bhakay-Tamhane, A. Sequeira R. Chidambaram ,Acta Cryst. C40 (1984) 1648-1651
36) Single-crystal neutron diffraction study of ferroelectric $Ba_{o.92}$ $Ca_{0.08}$ TiO_3, H Rajagopal, P U M Sastry, A Sequeira and P Ramasamy Bull. Mater. Sci., 17 (1994) 201-204.
37) Single-crystal neutron diffraction study of the structural phase transition in $Ba_{0:95}Ca_{0:05}TiO_3$, P U M Sastry, A Sequeira, H Rajagopal, B A Dasannacharya, S Balakumar, R Ilangovan and P Ramasamy, J. Phys.: Condens Matter 8 (1996) 2905-2913
38) Zinc (tris) thiourea sulphate (ZTS): A single crystal neutron diffraction study, P U Sastry, R Chitra, R. R. Choudhury and M Ramanadham, Pramana J. Phys. 63 (2004) 257-261
39) Single crystal neutron diffraction study of Triglycine Sulphate revisited R.R. Choudhury and R. Chitra, Pramana, 71 (2008) 911-915
40) Structural origin for the change of the order of ferroelectric phase transition in triglycine sulfate/selenatesystems Rajul Ranjan Choudhury and R Chitra J. Phys.: Condens. Matter 21 (2009) 335901
41) Prevention of depoling in TGS crystals by alanine substitution: An interpretation Based on Neutron Diffraction study R.R. Choudhury, R.Chitra, and M.Ramanadham Applied Physics A 74 (suppl.) (2002) S1667-S1669
42) Single-crystal neutron diffraction investigation on crystals belonging to the langasite family: A comparative study R. Chitra, R.R.Choudhury, Acta Crystallographica Section B: Structural Science 66(2010) 497-502
43) α-Nickel sulfate hexahydrate crystals: relationship of growth conditions, crystal structure and properties R. R. Choudhury, R. Chitra, I. P. Makarova, V. L. Manomenova, E. B.,Rudneva, A. E. Voloshin and M. V. Koldaeva, J. Appl. Cryst. 52 (2019) 1371–1377
44) Influence of N-H-O hydrogen bonds on the structure and properties of $(K_{1-x}(NH_4)_xH_2PO_4)$ proton glasses: A single crystal neutron diffraction study R.R Choudhury, R. Chitra**,** Journal of Physics Condensed Matter, 25 (2013) 075902

45) A single crystal neutron diffraction study on mixed crystal $(K)_{0.25}(NH_4)_{0.75}H_2PO_4$: tuning of short strong hydrogen bonds by ionic interactions, R.R Choudhury, R. Chitra. Bulletin of Materials Science 41 (2018) 8

46) Investigation of nuclear quantum effect on the hydrogen bonds of ammonium dihydrogen phosphate using single-crystal neutron diffraction and theoretical modelling R.R Choudhury,., R. Chitra, Pramana - Journal of Physics 91(2018) 53

47) Thiourea Doped Ammoniun Dihydrogen Phosphate: A Single Crystal Neutron Diffraction Investigation A.Jayarama, M.R.Suresh kumar, S M Dharmaprakash, R Chitra and R.R. Choudhury Pramana, 71 (2008) 905-910

48) Effect of cationic substitution on the double-well hydrogen-bond potential in $[K_{1-x}(NH_4)x]_3H(SO_4)_2$ proton conductors: A single-crystal neutron diffraction study, R.R. Choudhury, R. Chitra, E.V. Selezneva, I.P. Makarova, Acta Cryst. B 7 3(2017) 863-867

49) Deterioration of hydrogen-bonded superprotonic conductors belonging to $CsHSO_4–CsH_2PO_4–H_2O$ salt system: a single-crystal neutron diffraction investigation, R R Choudhury, R. Chitra, I P Makarova, E V Selezneva and V AKomornikov, Bull. Mater. Sci 44(2021) 108.

50) Investigation of hydrogen-bond network in bis(glycinium) oxalate using single-crystal neutron diffraction and spectroscopic studies, R. Chitra and R. R Choudhury, Acta Cryst. B63 (2007) 497–504

51) L-Histidine with nitric acid: A comparison of Crystal structures and Hirshfeld surfaces analysis Chitra, R., Choudhury, R.R., Rajan, R.V., Sajan, D., Kumar, M. Journal of Molecular Structure,1267 (2022) 133550

Neutron Conferences and Workshops

July 2023

Workshop - ILL Soft Matter Summer School
July 04-06, 2023, ILL, Grenoble, France
https://workshops.ill.fr/event/346/

Workshop – 29th Center for High Resolution Neutron Scattering (CHRNS) Summer School on Neutron Scattering
July 17-21, 2023, NIST, USA
https://www.nist.gov/ncnr/chrns/education-and-outreach/chrns-summer-school-neutron-scattering

August 2023

Conference - ICNPNS 2023: International Conference on Neutron Physics and Neutron Scattering
August 03-04, 2023, Montreal, Canada
https://waset.org/neutron-physics-and-neutron-scattering-conference-in-august-2023-in-montreal

Workshop - 25th National School on Neutron and X-ray Scattering
August 6-18, 2023, Oak Ridge National Laboratory, USA
https://neutrons.ornl.gov/nxs

Workshop - Röntgen-Ångström-Cluster (RÅC) International Summer School
August 20-27, 2023, Lüneburg, Germany
https://www.rac-school.org/

September 2023

Workshop - ESRF/ILL International Student Summer Programme on X-Ray and Neutron Science
September 03-29, 2023, ILL, Grenoble, France
https://www.esrf.fr/summerschool2023

Conference - ICNPNS 2023: International Conference on Neutron Physics and Neutron Scattering
September 20-21, 2023, Lisbon, Portugal
https://waset.org/neutron-physics-and-neutron-scattering-conference-%20in-september-2023-in-lisbon

Workshop - 25th JCNS Laboratory Course - Neutron Scattering 2023
September 04 – 15, 2023 Jülich/Garching, Germany
https://www.fz-juelich.de/en/jcns/expertise/conferences-and-workshops/labcourse/labcourse-2023/application

Workshop - Fundamentals of Neutron Spin Echo (NSE) Spectroscopy for Biology and Soft Matter
September 19-21, 2023, Gaithersburg, MD, USA
https://cns.che.udel.edu/2023-nse-workshop/

Workshop - Exploring the Dynamics in Soft Materials with Neutron Scattering
September 26-27,2023, Oak Ridge National Laboratory, USA
https://conference.sns.gov/event/371/

October 2023

Workshop - Trends and Perspectives in Neutron Scattering: Future Instruments at Pulsed Sources
October 09-12, 2023, Tutzing, Germany
https://www.fz-juelich.de/en/jcns/expertise/conferences-and-workshops/jcns-workshops/jcns-workshop2023

November 2023

Conference - International Conference on Synchrotron Radiation and Neutrons in Art and Archaeology
November 21–24, 2023, Pinakothek der Moderne, Munich
https://indico.frm2.tum.de/event/392/

December 2023

Conference - AOCNS 2023: Asia-Oceania Conference on Neutron Scattering
December 02–08, 2023, Royal Garden Hotel, Dongguan, China
http://aonsa.org/aocns/

March 2024

Workshop - HERCULES European School-Neutrons & Synchrotron Radiation for Science
March 2024, Grenoble, France
https://hercules-school.eu/

Neutron Scattering Society of India

(Registered No. Maharashtra State, Mumbai, 2011 GBBSD/1696)

(For Promotion of Neutron Scattering Research in India)

C/o Solid State Physics Division,
Bhabha Atomic Research Centre, Mumbai 400085

Phones: 91-22-25595376, 25593754, 25594307

Email:neutron@barc.gov.in; URL : http://www.nssi.org.in

Affix your PP size recent photograph here

*Application Form for Membership**

Name (in Capital letters)[$]: Prof/Dr/Ms/Mr **(Surname last)**	
Nationality:	**Date of Birth:** (dd/mm/yyyy)
Academic Qualification:	**Sex: M/F**
Profession:	**Neutron User Experience** (in yrs):
Nature of Present work:	
Affiliation: **Pin Code:**	**Residential Address:** **Pin Code:**
STD Code & Phone (O):	**STD Code & Phone (R):**
STD Code & FAX No.	**Mobile:**
Email-1:	**Email-2:**
[+]Details of Cheque/DD[+]: No.	**dated** **Bank:**
Endorsed by: (Either an existing member of NSSI or Head of the Affiliated Institute/University)	
Name & Designation	**Signature**
Date:	**Signature:**

*Life Membership fee: Rs. 1000/- (One thousand only)

[+]In favour of 'Neutron Scattering Society of India' payable at Mumbai

To: Secretary, ***Neutron Scattering Society of India***